

# Design and Testing of a Lobed Mixer for the Study of Mixing Enhancement in Reacting Flows

by

Thomas G. London

Ingénieur, École Centrale Paris, 1994  
D.E.A. de Combustion, École Centrale Paris, 1994

Submitted to the Department of Aeronautics and Astronautics in  
partial fulfillment of the requirements for the degree of

**Master of Science  
in Aeronautics and Astronautics at the  
Massachusetts Institute of Technology**

September 1995

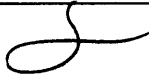
© 1995 Thomas G. London. All Rights Reserved.

The author hereby grants M.I.T. permission to reproduce and to distribute publicly paper and  
electronic copies of this document in whole or in part.


Signature of Author \_\_\_\_\_

Department of Aeronautics and Astronautics  
August 1995

Certified by \_\_\_\_\_

  
Professor Ian A. Waitz  
Thesis Supervisor

Accepted by \_\_\_\_\_

  
Professor Harold Y. Wachman  
Chairman, Department Graduate Committee

MASSACHUSETTS INSTITUTE  
OF TECHNOLOGY

SEP 25 1995

Aero

LIBRARIES



# Design and Testing of a Lobed Mixer for the Study of Mixing Enhancement in Reacting Flows

by

Thomas G. London

Ingénieur, École Centrale Paris, 1994

D.E.A. de Combustion, École Centrale Paris, 1994

Submitted to the Department of Aeronautics and Astronautics in partial fulfillment of the requirements for the degree of Master of Science in Aeronautics and Astronautics at the Massachusetts Institute of Technology

## Abstract

An existing experimental facility was modified to allow for the mixing enhancement associated with axisymmetric lobed mixers to be studied in reacting flows. A vertically-standing burner created two axisymmetric co-flowing streams of air and fuel upon which mixing enhancement could be performed. A turbulent, diffusive, momentum-driven flame burned downstream of the exit nozzle. The facility was resized and improved significantly to increase the flow rates and assure maximum safety. A lobed nozzle to be used with the facility was designed to study streamwise vorticity enhanced mixing. The facility was then tested for proper functioning. The performance of the lobed mixer was also tested, using oil flow visualization and total pressure surveys. The flow field along the nozzle and at the trailing edge was examined, and no boundary layer separation was found to occur. Finally, total pressure surveys were conducted downstream of the trailing edge to provide a qualitative characterization of the flow field from both the lobed mixer and a "baseline" non-lobed mixer. The lobed mixer was found to introduce large-scale streamwise vortices into the flow.

Thesis Supervisor : Ian A. Waitz  
Professor of Aeronautics and Astronautics

# Acknowledgments

The completion of this thesis would have been impossible without the help and the support of numerous persons. Among them, I wish to thank in particular :

**Professor Ian A. Waitz** for offering me the opportunity to work on this project, for providing a very dynamic and challenging environment, and for his precious assistance throughout the project,

**Professor Edward M. Greitzer** for his helpful suggestions and constructive criticism,

**Richard Perdichizzi, Bill Ames** and **Jim Letendre** for their priceless help and experience,

**Jan Krasnodebski, Julian Sell, Dave Tew** and **Dave Underwood** for patiently answering all my silly questions,

**Denis Houles, Olivier Piepsz, Jérôme Gonichon** and the rest of the “Maison du Bonheur” for making this year a great one (did Parker release a rating ?),

**Marius Paraschivoiu**, for keeping me on the right track, whether it was paved with equations, bottles of wine or white sand,

**Fiero** and **Ralph** for providing the transportation,

**Dr. Gérard London** and **Dr. Alena London**, my parents, for their unalterable support and for the partial funding provided for my Master’s studies,

The **George Lurcy Foundation** for their partial funding of my Master’s,

**Francina van Boxtel** for the years passed and the years to come.



# Contents

<b>Abstract .....</b>	<b>3</b>
<b>Acknowledgements .....</b>	<b>4</b>
<b>Table of Contents.....</b>	<b>5</b>
<b>List of Figures.....</b>	<b>8</b>
<b>List of Tables .....</b>	<b>10</b>
<b>List of Symbols .....</b>	<b>11</b>
<b>1. Introduction.....</b>	<b>13</b>
1. 1. Introduction .....	13
1. 2. Background.....	14
1. 3. Objectives and approach.....	15
1. 4. Overview of the thesis .....	15
<b>2. Facility design .....</b>	<b>19</b>
2. 1. Review of the previously existing facility .....	19
2. 1. 1. Design motivation .....	19
2. 1. 2. Features of the previously existing facility.....	20
2. 2. Resizing of the facility.....	21
2. 2. 1. Flow rates .....	22
2. 2. 1. a. Fuel lines.....	22
2. 2. 1. b. Air line .....	24
2. 2. 2. Pressure losses .....	24
2. 2. 3. Minimum time span for testing.....	26
2. 2. 4. Safety .....	27

2. 3. Changes implemented on the facility .....	27
2. 3. 1. Modified features.....	28
2. 3. 2. New operating procedures .....	30
<b>3. Lobed nozzle design.....</b>	<b>35</b>
3. 1. Theoretical background .....	35
3. 1. 1. Vorticity in a shear layer .....	35
3. 1. 2. Lobed mixer enhancement.....	36
3. 2. Preliminary design considerations .....	37
3. 2. 1. a. Fuel composition.....	38
3. 2. 1. b. Geometry of the “baseline” configuration.....	39
3. 3. Flowfield constraints.....	40
3. 3. 1. Introduction of streamwise vorticity.....	40
3. 3. 2. Boundary layer blockage .....	41
3. 3. 2. a. Determination of the design fuel composition.....	41
3. 3. 2. b. Pressure gradient along the nozzle .....	42
3. 3. 2. c. Displacement thickness .....	43
3. 3. 3. Flame holding .....	47
3. 4. Structural constraints : thermal stresses.....	47
3. 4. 1. a. Temperature profile in the metal.....	48
3. 4. 1. b. Maximum thermal stress .....	51
3. 5. Lobed mixer geometry.....	52
<b>4. Experimental approach and results .....</b>	<b>61</b>
4.1. Experimental approach.....	61
4.1.1.a. Evaluation of the facility.....	62
4.1.1.b. Examination of the flow along the nozzle .....	63
4.1.2. Survey of the flow field .....	63
4.1.2.a. Experimental approach .....	63
4.1.2.b. Experimental apparatus .....	64
4.1.2.c. Uncertainty .....	65
4.1.2.d. Signal-to-Noise ratio.....	66
4.2. Results .....	66
4.2.1. Evaluation of the facility .....	66
4.2.2. Examination of the flow along the nozzle .....	69
4.2.2.a. Oil flow visualization.....	69
4.2.2.b. Total pressure measurements.....	69
4.2.3. Qualitative survey of the flow field .....	70
<b>5. Conclusions and Recommendations .....</b>	<b>79</b>
<b>References .....</b>	<b>81</b>
<b>Appendix A : New instrumentation and hardware specifications.....</b>	<b>85</b>

**Appendix B : Boundary layer growth along the nozzle .....87**  
**Appendix C : Thermal stresses, complete results.....89**  
**Appendix D : Corrections on helium flow rates .....91**

# List of Figures

Figure 1.1 :	Lobed mixer .....	17
Figure 2.1 :	Photographs of the experimental facility .....	30
Figure 2.2 :	Facility control diagram .....	31
Figure 2.3 :	Facility control panel .....	32
Figure 2.4 :	Annular burner (vertical section) .....	33
Figure 3.1 :	Spanwise vorticity about a lobed mixer .....	53
Figure 3.2 :	Formation of streamwise vorticity in a lobed mixer.....	53
Figure 3.3 :	Dimensions of the non-lobed nozzle .....	54
Figure 3.4 :	Dimensions of the co-flow nozzle .....	54
Figure 3.5 :	Boundary layer blockage in a lobed mixer .....	55
Figure 3.6 :	Thermal expansion of the lobe walls .....	55
Figure 3.7 :	Heat transfer to a lobe wall, practical situation .....	56
Figure 3.8 :	Model for the heat transfer to a lobe wall.....	56
Figure 3.9 :	Temperature profile in the lobes ( $z=0$ at the inlet of the lobes).....	57
Figure 3.10 :	Lobed mixer, front view.....	58
Figure 3.11 :	Lobed mixer, upper view.....	59
Figure 3.12 :	Lobed mixer, cross sections .....	59

Figure 3.13 :	Lobed and non-lobed mixers.....	60
Figure 4.1 :	Flammability limit .....	72
Figure 4.2 :	Oil flow visualization of the core flow at $15 \text{ m.s}^{-1}$ (partial vue) .....	72
Figure 4.3 :	Total pressure along the radial axis of an external lobe, at 0.02" downstream of the trailing edge, lobed mixer, $r=1.4$ .....	73
Figure 4.4 :	Total pressure along the radial axis of an internal lobe, at 0.02" downstream of the trailing edge, lobed mixer, $r=1.4$ .....	73
Figure 4.5 :	Total pressure along a radius, at 0.02" downstream of the trailing edge, non-lobed mixer, $r=1.4$ .....	74
Figure 4.6 :	Dynamic pressure, lobed mixer at $z=1''$ for $r=0.74$ .....	74
Figure 4.7 :	Dynamic pressure, lobed mixer at $z=2''$ for $r=0.74$ .....	75
Figure 4.8 :	Dynamic pressure, non-lobed mixer at $z=2''$ for $r=0.74$ .....	75
Figure 4.9 :	Dynamic pressure, lobed mixer at $z=1''$ for $r=1.53$ .....	76
Figure 4.10 :	Dynamic pressure, lobed mixer at $z=2''$ for $r=1.53$ .....	76
Figure 4.11 :	Dynamic pressure, non-lobed mixer at $z=2''$ for $r=1.53$ .....	77

# List of Tables

Table 2.1 : Pressure levels and burner exit velocity for ¼" lines ..... 25

Table 3.1 : Boundary layer growth across the nozzle ..... 46

Table 3.2 : Maximum thermal stress within the lobed mixer ..... 52

Table 4.1 : Operating range of the facility..... 67

# List of Symbols

## Roman Letters

<i>A</i>	<i>Area (m<sup>2</sup>)</i>
<i>Bi</i>	<i>Biot number</i>
<i>D</i>	<i>Diameter (m)</i>
<i>f</i>	<i>Friction coefficient</i>
<i>g</i>	<i>Gravitational acceleration (m.s<sup>-2</sup>)</i>
<i>h</i>	<i>Heat transfer coefficient</i>
<i>H</i>	<i>Shape factor</i>
<i>H</i>	<i>Lobe height (m)</i>
<i>k</i>	<i>Thermal conductivity (J.m<sup>-2</sup>K<sup>-1</sup>)</i>
<i>K</i>	<i>Loss coefficient</i>
<i>l</i>	<i>Length (m)</i>
<i>Nu</i>	<i>Nusselt number</i>
<i>m</i>	<i>Mass flow (kg.s<sup>-1</sup>)</i>
<i>P</i>	<i>Pressure (Pa, or psi ; 10<sup>5</sup> Pa = 14.7 psi)</i>
<i>Pr</i>	<i>Prandtl number</i>
<i>r</i>	<i>Velocity ratio (m.s<sup>-1</sup>)</i>
<i>Ra</i>	<i>Rayleigh number</i>
<i>Re</i>	<i>Reynolds number</i>
<i>T</i>	<i>Temperature</i>
<i>U</i>	<i>Free stream velocity (m.s<sup>-1</sup>)</i>
<i>v</i>	<i>Velocity (m.s<sup>-1</sup>)</i>
<i>V</i>	<i>Voltage (volts)</i>
<i>V</i>	<i>Volume (m<sup>3</sup>)</i>
<i>V̇</i>	<i>Volumetric Flowrate (m<sup>3</sup>.s<sup>-1</sup>, or SLPM, or SCFM)</i>
<i>x, y</i>	<i>Molar Fraction</i>
<i>z</i>	<i>Axial coordinate (m)</i>

## Greek Letters

$\alpha$	<i>Ramp angle (rad)</i>
$\Gamma$	<i>Circulation (<math>m^2.s^{-1}</math>)</i>
$\delta^*$	<i>Displacement thickness (m)</i>
$\delta_2$	<i>Momentum thickness (m)</i>
$\delta_3$	<i>Energy thickness (m)</i>
$\lambda$	<i>Lobe wavelength (m)</i>
$\mu$	<i>Dynamic viscosity (<math>kg.m^{-1}.s^{-1}</math>)</i>
$\nu$	<i>Kinematic viscosity (<math>m^2.s^{-1}</math>)</i>
$\rho$	<i>Density (<math>m^3.s^{-1}</math>)</i>
$\sigma$	<i>Standard deviation</i>
$\tau$	<i>Characteristic time</i>
$\phi$	<i>Equivalence ratio</i>

## Subscripts

<i>1</i>	<i>Burner nozzle inlet section, co flow</i>
<i>1c</i>	<i>Burner nozzle inlet section, core flow</i>
<i>2</i>	<i>Inlet cross-section of the lobed section of the burner nozzle, co flow</i>
<i>2c</i>	<i>Inlet cross-section of the lobed section of the burner nozzle, core flow</i>
<i>3</i>	<i>Burner nozzle co flow exit section, co flow</i>
<i>3c</i>	<i>Burner nozzle core flow exit section</i>
<i>alc</i>	<i>Manometer alcohol</i>
<i>bottle</i>	<i>Compressed gas bottle</i>
<i>core</i>	<i>Core flow</i>
<i>co</i>	<i>Co flow</i>
<i>dyn</i>	<i>Dynamic</i>
<i>ext</i>	<i>External</i>
<i>forced</i>	<i>Forced convection</i>
<i>H<sub>2</sub></i>	<i>Hydrogen flow</i>
<i>He</i>	<i>Helium flow</i>
<i>in</i>	<i>Input</i>
<i>mean</i>	<i>Average between co flow and core flow</i>
<i>N<sub>2</sub></i>	<i>Nitrogen flow</i>
<i>natural</i>	<i>Natural convection</i>
<i>out</i>	<i>Output</i>
<i>sp</i>	<i>spanwise</i>
<i>st</i>	<i>streamwise</i>
<i>std</i>	<i>Under standard conditions</i>
<i>total</i>	<i>Tube portion where H<sub>2</sub> and N<sub>2</sub> are already mixed and before inlet into the burner</i>
<i>tubing</i>	<i>Tubing (gas supply)</i>



# 1. Introduction

## 1. 1. Introduction

In most combustion processes, mixing is a crucial factor. How quickly and how thoroughly the fuel and the oxidant are mixed greatly affects critical parameters such as combustion efficiency, heat release rate, pollutant formation and combustor size.

One technology that has recently received considerable attention for enhancing the mixing between co-flowing streams is the lobed mixer (cf. Figure 1.1). This type of device has been used in recent turbofan engine configurations at the interface between the core air and the bypass air ([15], [19]) where fast and complete mixing is required.

Using a lobed mixer increases the initial interfacial area between the two co-flowing fluids and introduces large-scale streamwise vorticity into the flow. Both of these factors increase the area of the interface through which the mixing occurs and enhance the mixing process.

The objectives of the work presented in this thesis are :

- to build and test a facility which will allow the study of the mixing enhancement associated with lobed mixers in reacting flows,
- to design a lobed mixer suitable for the study,
- to provide a preliminary characterization of the lobed mixer flowfield.

## 1. 2. Background

Early investigations of lobed mixers focused on the study of turbofan exhaust sections, and the mixing between the core and the bypass air ([10], [6], [11], [20], [1]). These studies showed that lobed mixers can be used to enhance mixing with relatively low total pressure loss. The lobe penetration angle,  $\alpha$ , defined in Figure 1.1 was found to have a strong impact on the mixing enhancement, provided the flow does not separate from the surfaces of the lobes. The lobe penetration angle is directly related to the shed streamwise circulation. Separation increases the pressure losses and reduces the mixing effectiveness. Other applications of lobed mixers have also been investigated. For instance, Presz, *et al.* [22] reported a significant increase in ejector pumping performance when lobed mixers are used instead of conventional flat splitter plates.

The mixing process in lobed mixers was found to be related to :

1. the normal vorticity typical of a planar shear layer,
2. the streamwise vorticity generated by the lobed geometry,
3. the increase in the initial interfacial area between the two flows.

Indeed, while normal vorticity is inherent to mixing in a shear layer, streamwise vorticity has been identified ([2], [22], [8]), along with the increase in interfacial area, as the main agents which enhance mixing in lobed mixer flow. The relative importance of the increase in initial interfacial area and the introduction of streamwise vorticity on the mixing augmentation has been investigated by Manning [14], who found the contribution of streamwise vorticity to increase with the velocity ratio between the two flows. More recently, Qiu [23] identified the stretching of the mean cross-flow interface as the main mechanism through which streamwise vorticity enhances mixing. Waitz and Underwood [32] compared the mixing downstream of a lobed mixer to that of a flat plate with varying amounts of heat release. They found that the lobed mixer flow was less sensitive to the detrimental effects of heat release than the planar shear layer.

Nevertheless, most of the research on lobed mixer devices has focused largely on planar, non-reacting flows, and the performance of axisymmetric lobed mixers in reacting flows

remains to be studied. The critical issues include the influence of heat release on the mixing performance and the impact of high strain rates on the chemical reactions taking place at the interface between the fuel and the oxidizer.

### **1. 3. Objectives and approach**

The purpose of the current project is to provide a means to experimentally compare the mixing augmentation from a lobed mixer in cold and reacting flow. An experimental facility constructed by McGrath [16] was used to test both a lobed and a non-lobed (“baseline”) configuration. Experiments were conducted in cold-flow (with a co-flow of air and of a helium-nitrogen mixture) as well as in reacting flow (by replacing the helium by hydrogen). The velocity ratio between the air and fuel flows was also varied.

To support this effort the following tasks were completed and are discussed in this thesis:

- The experimental facility was modified significantly to increase the flow rates and allow the mixing enhancement associated with axisymmetric lobed mixer in reacting flows to be studied,
- A lobed mixer was designed to be used with the facility,
- Oil flow visualizations of the flow along the lobed nozzle were performed, as well as a survey of the structure of the shear layer from both the lobed mixer and a “baseline” non-lobed mixer. This survey employed time-averaged total pressure measurements to outline the flow patterns downstream of the lobed mixer, in order to verify the performance of the lobed mixer that was designed.

### **1. 4. Overview of the thesis**

Modifications to the reacting flow facility are discussed in Chapter 2. The design of the lobed nozzle is presented and discussed in Chapter 3. The experimental approach and

the results of the survey of the flow are then presented in Chapter 4. Finally, recommendations for improvements and future investigations are made in Chapter 5.

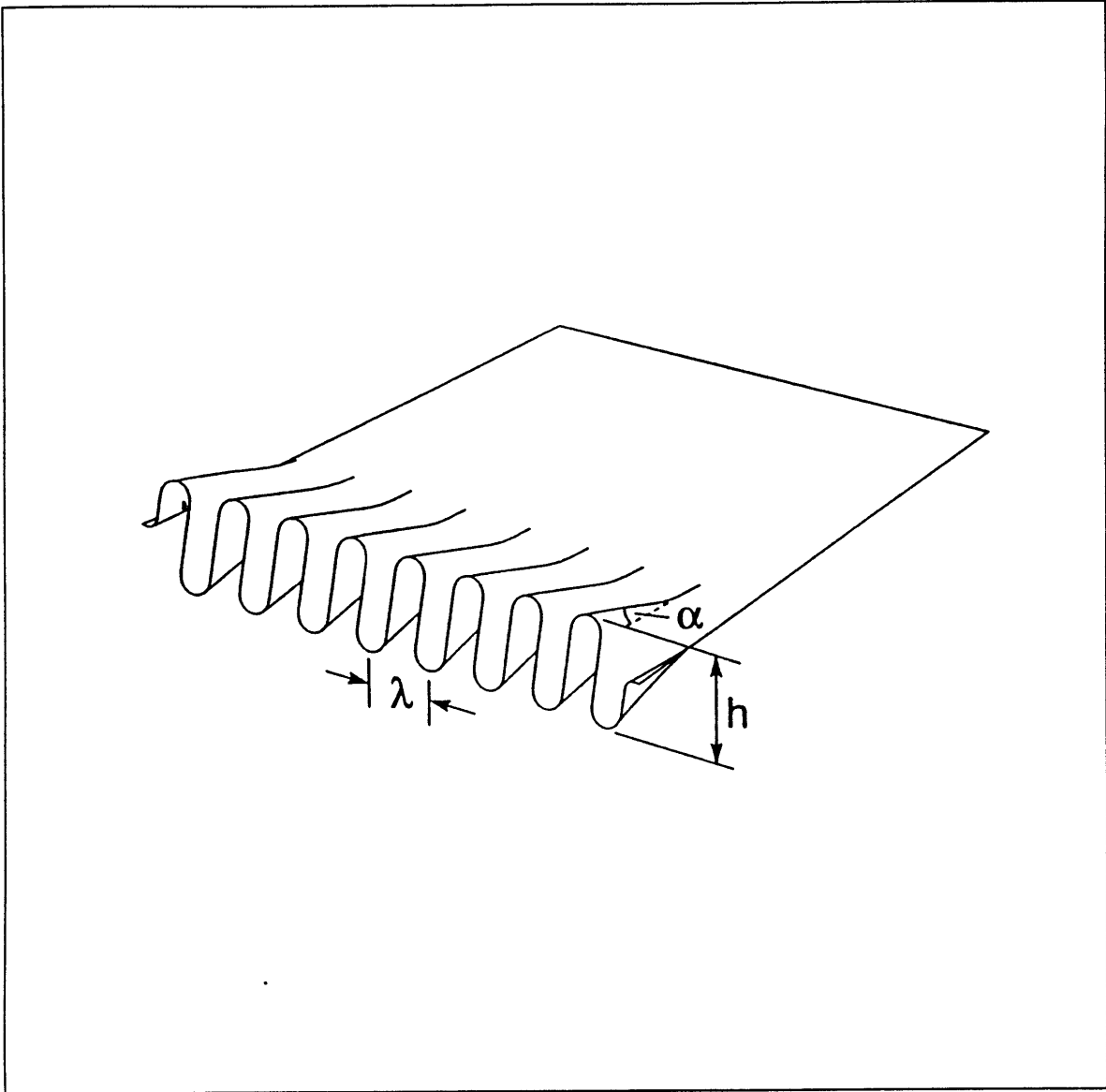


FIGURE 1.1 : LOBED MIXER



## 2. Facility design

The first step of this study was to modify the facility to increase the flow rates and to provide an easier, safer control system. In this chapter, the earlier characteristics of the facility are first presented and reviewed. Then, the design changes that were investigated are listed and discussed. Finally, the details of the changes that were implemented on the facility are presented.

### 2. 1. Review of the previously existing facility

#### 2. 1. 1. Design motivation

The ultimate objective of the project is to investigate mixing enhancement associated with lobed mixers in axisymmetric reacting flows. The experimental facility built for this purpose has to generate a proper flowfield upon which mixing augmentation can be performed. A vertically standing burner showed on Figure 2.1 serves this purpose, creating two axisymmetric co-flowing streams of air and fuel.

Since most of the applications which could benefit from lobed mixing technology (turbojet afterburners, gas turbine and ramjet combustors, etc.) operate with turbulent diffusion flames, the burner must generate a turbulent diffusion flame to reproduce the reacting flows to be studied. As a guideline, a critical Reynolds number of 3500 is used as the criterion for the transition to turbulent conditions. Further, in most practical applications of lobed mixers, buoyancy forces are small compared to momentum forces.

Hence, as discussed in McGrath [16], the burner must generate a turbulent, momentum-driven flame, to match the practical conditions as closely as possible. However, the flow rates available in the facility were insufficient to reach such conditions. Thus the facility had to be resized.

## **2. 1. 2. Features of the previously existing facility**

The design of the facility was conducted by McGrath [16]. This design was used as a basis for the present work and should be consulted for a detailed description of the facility. An annular burner, shown in Figure 2.2 is fed by controllable flow rates of air and of a hydrogen/nitrogen mixture.

The main features of the system are:

- the facility can be operated by a single person, from a separate room, through the use of an extensive control panel shown in Figure 2.3. The control of the system includes an automatic ignition system, commands controlling the air, hydrogen and nitrogen flows.
- an efficient ventilation system rapidly evacuates burned and unburned gases from the test cell,
- a reliable flame detection system turns off the system in case of an ignition fault, to avoid hydrogen from spreading into the test cell,
- since the aim is to compare the results with non-reacting flow results under an array of different conditions, the flame needs to have broad flammability limits. Hence, for flame stability and flammability reasons, hydrogen was chosen as a fuel. In addition, a specified amount of nitrogen can be mixed with the hydrogen before the mixture enters the burner. Using nitrogen as a diluent allows the rate of heat release in the mixing layer to be varied,
- an annular, vertically-standing burner, shown in Figure 2.4, was built. This burner was designed to create a turbulent momentum-driven diffusion flame between two co-flowing streams of air and fuel. It allows the operator to vary the vorticity in the mixing process by changing the shape of the nozzle (lobed or non-lobed). The



operator can also control the level of turbulence of the flow exiting the burner by adding or removing turbulence-controlling screens inside the burner,

- appropriate operating procedures have been elaborated to insure maximum safety during each run.
- The diameter of the “baseline” core nozzle was chosen to be 1” The outer diameter (diameter of the co-flow exit nozzle) is 5.5”. This choice of diameters resulted from a trade-off between the size of the shear layer (reducing the diameter would reduce the size of the structures to be measured, causing potential resolution problems) and the capacity of the gas supply (increasing the diameter would require higher flow rates for the same exit velocity). Also, to avoid separation problems, the cross-sectional area of both the core and the co-flow decrease axially along the nozzle, creating a favorable pressure gradient (see section 3. 2. 1 for more details).
- The hydrogen and nitrogen are stored in compressed gas bottles. The air is supplied through a laboratory-wide oil-free compressed air line, which can deliver a maximum of 0.75 *lbs/s* of air at 100 *psi*.
- The flow rates can be varied as follows :
  - Hydrogen flow : 0 to 30 *SLPM* (Standard Liter per Minute)
  - Nitrogen flow : 0 to 30 *SLPM*
  - Air flow : 0 to 50 *SCFM* (Standard Cubic Feet per Minute), i.e. 0 to 1415 *SLPM*.

Provided that the air flow exit area is  $A_3 = 1.48 \times 10^{-2} m^2$  and the fuel exit area is  $A_{3c} = 5.07 \times 10^{-4} m^2$ , this corresponds to a range of air to fuel velocity ratio from approximately 0.3 to 3.

Furthermore, in order to have a turbulent momentum-driven flame in all cases (as discussed in McGrath’s thesis [16], pp. 26, 27 and 30), the exit velocities have to be higher than 4 *m.s<sup>-1</sup>* (cf. Figure 2.12 in McGrath [16]). Yet, the flow rates available yield exit velocities of the order of 1 *m.s<sup>-1</sup>*. Hence, the facility required resizing.

## 2. 2. Resizing of the facility

To provide an effective range of velocity ratios from 0.3 to 3 while exceeding  $4 \text{ m.s}^{-1}$  in all configurations, the exit velocities of each flow have to cover a range of approximately 4 to  $12 \text{ m.s}^{-1}$ . For both the fuel and the air flows, the design velocity was  $v_{3c} = 15 \text{ m.s}^{-1}$  to provide an operating margin. Since the flow rates of air and fuel must be sufficient to reach  $15 \text{ m.s}^{-1}$ , the requirements for the air and fuel lines were changed. These changes are discussed in the following section.

### 2. 2. 1. Flow rates

The flow rates needed to reach the required exit flow velocities are the main parameters that set the size of the flow-controlling apparatus (such as flowmeters, 2-way solenoid valves, etc.) which have to be installed in the lines. The flow rates are therefore crucial to the sizing of the facility. This section details the calculation of the required flow rates for both the fuel and the air lines.

#### 2. 2. 1. a. Fuel lines

Assuming that all gases behave like ideal gases, the molar volumes of the two gases are equal since they are under the same conditions (same pressure and temperature). Hence, the volume fractions in the mixture are equal to the molar fractions. Therefore, the density of the mixture of  $\text{H}_2$  and  $\text{N}_2$  is :

$$\rho_{total} = x \cdot \rho_{H_2} + y \cdot \rho_{N_2} \quad (2.1)$$

where  $x$  and  $y$  are the molar fractions of  $\text{H}_2$  and  $\text{N}_2$ . It is assumed that all gases are incompressible.

The cross-sectional area of the tubing is the same everywhere in the fuel lines ( $A_{total}=A_{H_2}=A_{N_2}=A$ ). Therefore, by conservation of the mass flow for each species :

$$\dot{m}_{total} = \rho_{total} A v_{total} = (x \cdot \rho_{H_2} + y \cdot \rho_{N_2}) A v_{total} = \dot{m}_{H_2} + \dot{m}_{N_2} \quad (2.2)$$

i.e.

$$\dot{m}_{H_2} = xv_{total}\rho_{H_2}A \quad (2.3)$$

and

$$\dot{m}_{N_2} = yv_{total}\rho_{N_2}A \quad (2.4)$$

In terms of volumetric flow rates, this gives :

$$\dot{V}_{H_2} = \frac{\dot{m}_{H_2}}{\rho_{H_2}} = xAv_{total} = x\dot{V}_{total} \quad (2.5.a)$$

$$\dot{V}_{N_2} = y\dot{V}_{total} \quad (2.5.b)$$

For  $v_{3_c} = 15 m.s^{-1}$  and  $A_{3_c} = \frac{\pi}{4}D_{core}^2 = 5.067 \times 10^{-4} m^2$  one gets :

$$\dot{V}_{total} = A_{total}v_{total} = A_{3_c}v_{3_c} = 7.6 \times 10^{-3} m^3.s^{-1} \quad (2.6)$$

Since the heat radiated from the flame should not increase the temperature in the test cell over 120°F, and since the Reynolds number should always be over 3500, McGrath [16] determined that the upper limit in terms of hydrogen fraction in the mixture is :

$$x < 0.86 \quad (\text{i.e. } y > 0.14)$$

Increasing the mass fraction of hydrogen over 0.86 would yield unacceptable Reynolds number and cell temperature.

Using these values the maximum flow rate needed can be calculated :

- for H<sub>2</sub> :  $\dot{V}_{H_2} = x_{max}\dot{V}_{total} = 6.5 l.s^{-1} = 392 SLPM$
- for N<sub>2</sub> : in consideration of the value of the maximum H<sub>2</sub> flow rate, the N<sub>2</sub> line was sized to provide up to 300 SLPM.

Most of the equipment installed on the fuel lines was not appropriate for such flow rates, and had to be changed. Namely, the pressure regulators, solenoid valves, check valves, flowmeters, manual closing valves, particle filters were changed. The features of the new equipment are presented in Appendix A.

### 2. 2. 1. b. Air line

For the air line :

$$A_3 = \frac{\pi}{4} (D_{co}^2 - D_{core}^2) = 1.48 \times 10^{-2} m^2 \quad (2.7)$$

where  $D_{co}$  and  $D_{core}$  designate respectively the diameter of the co-flow cylinder and the core flow cylinder.

And since  $v_3 = 15 m.s^{-1}$ , this yields :

$$\dot{V}_3 = A_3 v_3 = 2.22 \times 10^{-1} m^3 .s^{-1} = 1.3 \times 10^4 SLPM = 470 SCFM$$

Once again, some of the air-controlling equipment installed in the facility was not appropriate. For the air line, the flowmeter was changed. The features of the new flowmeter are detailed in Appendix A.

### 2. 2. 2. Pressure losses

The pressure losses across the fuel lines (hydrogen and nitrogen) were estimated, to determine the pressure level required to drive the desired flow rate through the lines. At the exit of the regulators (which control the flow exiting the bottles), 2-way solenoid valves rated to 200 *psi* are used, and it is therefore not advisable to exceed pressure levels higher than approximately 200 *psi*.

The pressure losses occurring through the lines can be written as the sum of the losses due to the friction along the tubes and the losses occurring through each flow-controlling device (flowmeters, valves, junctions, filters, ...) :

$$\Delta P = \Delta P_{tubing} + \sum_i \Delta P_i \quad (2.8)$$

where each integer  $i$  refers to a flow-controlling device.

Equation (2.8) can be detailed [7] :

$$\Delta P = -f \frac{l}{D} \rho \frac{v^2}{2} + \frac{\rho}{2} \sum_i K_i v^2 \quad (2.9)$$

where  $f$  is the friction coefficient of the inner walls of the tubing,  $D$  is the diameter of the tubing, and  $K_i$  are the loss coefficients for each flow-controlling device and each change in the inner geometry of the tubing (contractions, T-intersections, elbows, etc.).

In addition :

$$v = \frac{\dot{V}}{A} \propto \frac{\dot{V}}{D^2} \quad (2.10)$$

Hence, for a given tube diameter, the pressure losses scale like  $\dot{V}^2$ . Determining the pressure losses for a given exit velocity will indicate whether using the same installation with roughly 10 times higher flow rates (as is intended) is possible.

The dynamic pressure at the exit of the burner was measured using a pitot tube linked to a pressure transducer. The uncertainty of this measure is of the order of 0.5 Pa (taking into account the reading uncertainty). The upstream pressure was read on the gas regulator, at the exit from the compressed bottle (the uncertainty of this second measure is roughly 10 psi, taking into account the reliability of the indication and the reading uncertainty).

The exit velocity was calculated using the dynamic pressure in the exit free jet :

$$v_3 = \sqrt{\frac{2P_{dyn}}{\rho_{N_2}}} \quad (2.11)$$

The results are shown on Table 2.1.

	Total Pressure (in Pa) @ exit of N <sub>2</sub> regulator	
	(8.3 ± 0.7) × 10 <sup>5</sup>	(15.9 ± 0.7) × 10 <sup>5</sup>
Dynamic Pressure (in Pa) in the exit free jet	11 ± 5	37 ± 5
Exit Velocity (in m.s <sup>-1</sup> )	4 ± 1	8 ± 1

TABLE 2.1 : PRESSURE LEVELS AND BURNER EXIT VELOCITY FOR ¼" LINES

These results show that reaching the required exit velocities ( $\cong 15 \text{ m.s}^{-1}$ ) would require increasing the pressure at the exit from the regulators to unacceptable levels (much

higher than 200 *psi*). Therefore, the lines could not be used as they were. Thus, the tubing was upgraded to ½" outer diameter (instead of ¼") and the flow-controlling devices were changed to ½"-section higher capacity apparatus (cf. Appendix A for details).

Equations (2.9) and (2.10) show that, for a given flow rate, the pressure losses decrease like the diameter of the duct squared. Hence, doubling the diameter should decrease the pressures losses sufficiently to reach exit velocities of the order of 15 *m.s*<sup>-1</sup> without an upstream pressure in excess of 200 *psi*.

### 2. 2. 3. Minimum time span for testing

The increase in the flow rates also raises the problem of the capacity of the compressed gas bottles used as nitrogen and hydrogen tanks. Because of the high flow rates, those bottles will rapidly discharge, and one has to make sure that the time available for each run before the bottles are empty is sufficient.

The volume and pressure of each bottle is :

$$\dot{V}_{bottle} \cong 3.7 \times 10^{-2} m^3 \text{ and } P_{bottle} \cong 2500 \text{ psi} = 170 \text{ atm}$$

Therefore, the volume occupied by the gas in the bottle under standard conditions can be estimated as follows :

$$V_{std} = \frac{P_{bottle}}{P_{std}} V_{bottle} = 6.3 m^3 \quad (2.12)$$

The characteristic time for the complete discharge of a bottle is :

$$\tau = \frac{V_{std}}{\dot{V}_{gas}} \quad (2.13)$$

And the highest flow rate reached for bottle-stored gases will determine the limiting test time available. The maximum flow rate is  $\dot{V}_{H_2} \cong 400 \text{ SLPM}$ , which gives :

$$\tau = \frac{V_{std}}{\dot{V}_{H_2}} \cong 15 \text{ minutes}$$

This time is sufficient to allow multiple measurements of the flame and should be adequate for the expected testing procedures (e.g. cross-plane surveys of the flow using laser diagnostics).

## 2. 2. 4. Safety

The use of hydrogen gas in the facility raises numerous safety issues. The most significant hazards associated with the use of hydrogen are :

- H<sub>2</sub> gas undetectability,
- quasi-undetectability of a clean H<sub>2</sub>-Air flame,
- wide flammability limits (the H<sub>2</sub>-Air mixture is flammable for H<sub>2</sub> composition from 4% to 75% in volume). H<sub>2</sub> build up in the test cell must be prevented,
- ignition of H<sub>2</sub>-Air mixture at very low energy input (0.02 mJ at 1 atm, i.e. 1/10 of what is required for a gasoline flame mixture). Hence, any potential sparks must be avoided in the wiring,
- low viscosity and molecular weight of H<sub>2</sub>. The system will therefore be susceptible to leakage problems.

To minimize the danger for the operator, the control of the whole system can be accomplished from a separate room. Ignition, control of the flow rates, purges, regular and emergency stops do not require the operator to get exposed to hydrogen. Moreover, a complete purge of the hydrogen line including the regulator can be performed prior to any hydrogen bottle change, to avoid unnecessarily exposing the operator.

Improvements were also made on the safety features of the facility. These improvements are discussed in the next section.

## 2. 3. Changes implemented on the facility

This section presents the changes that were implemented on the facility, as well as the corresponding operating procedures. Most of these changes were made on already existing features, but some new features were also installed.

### 2. 3. 1. Modified features

As previously mentioned, the hydrogen and nitrogen lines were upgraded to ½" tubing. When necessary, flow-controlling devices were also upgraded (cf. Appendix A for the features of the new equipment).

Some of the features of the control box have been improved :

- The display of the nitrogen-feed and air-feed functions was changed to clearly show its status (cf. Figure 2.3). For each gas, a separate button corresponds to each of the ON or OFF positions. In addition, the air-feed and nitrogen-feed are now being reset whenever the system is shut down (previously, if the air-feed or the nitrogen-feed were operating during shut-down, they would restart as soon as the system is restarted).
- A "hydrogen regulator purge" function has been implemented. Before any hydrogen bottle change, the operator can purge the hydrogen regulator by pressing a button on the control panel. This procedure also purges the hydrogen relief lines, since the excess gas is evacuated through the relief valves.
- The possibility of running cold-flow tests has also been implemented. Previously, the system did not allow the experiments with non-reacting gases (using helium instead of hydrogen), since it would shut down if no flame was detected ("ignition fault" sequence). An aircraft safety switch has been implemented (inside the control box to avoid unintentionally switching to ON during a run involving hydrogen) to disable the ignition fault sequence (this switch is labeled "controller bypass"). Hence, the system can now be run without a positive response of the flame detector. Also, another switch has been installed on the ignition power supply, to disconnect the ignition system, since it is not used during cold flow testing.



- Finally, a pressure gage was installed in the fuel line, just before the flash arrestor (i.e. about 3 feet before the inlet of the burner), to verify the existence of a flow through the lines during purges. This assures the operator that the purge is taking place.

### 2. 3. 2. New operating procedures

The potential danger associated with the *cold-flow testing* function calls for strict operating procedures. Leaving the cold-flow switch ON when going back to hydrogen runs would indeed mean that in case of an ignition fault, the system would pump unburned hydrogen into the test cell without detecting it. This section lists the steps to follow whenever running cold-flow experiments (the control panel is shown on Figure 2.3).

1. If running, stop the system (by pressing the “stop” button),
2. Close the hydrogen bottle and replace it by helium if necessary (purge the hydrogen regulator following the procedure described by McGrath [16]),
3. Turn the switch on the back of the ignition system power supply to the “ignition OFF” position,
4. Turn the “ignition fault bypass” switch (inside the control box) to the ON position,
5. Hit the “purge” button,
6. Hit the “start” button,
7. Run the experiment,
8. Hit the “stop” button when done,
9. Switch the “ignition fault bypass” back to OFF,
10. Switch the ignition power supply back to ON,
11. Reinstall and reopen the hydrogen bottle.

A more general “check list” covering the standard procedures is presented in McGrath [16]. It should be reviewed whenever starting the facility to insure maximum safety.

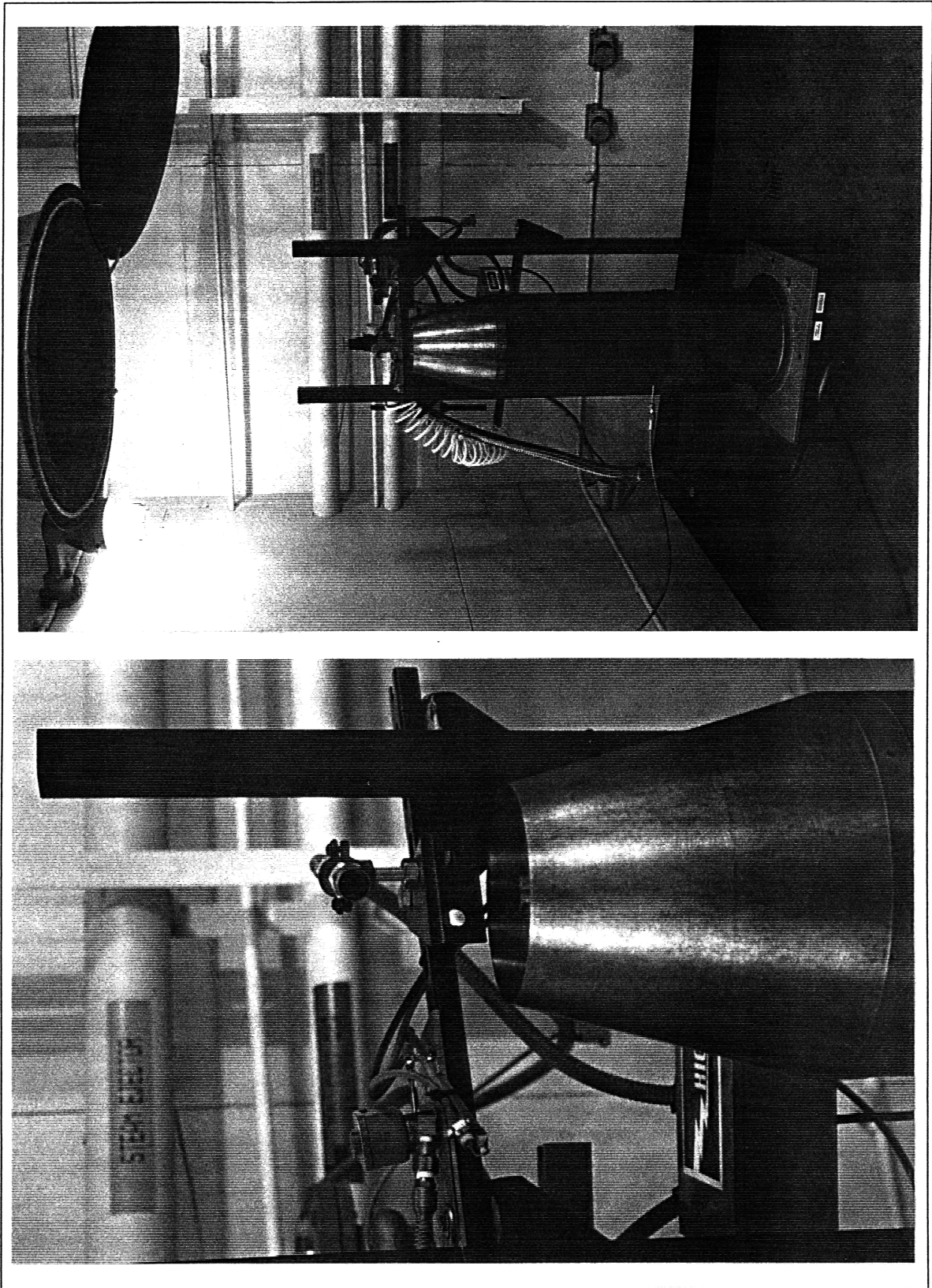


FIGURE 2.1 : PHOTOGRAPHS OF THE EXPERIMENTAL FACILITY

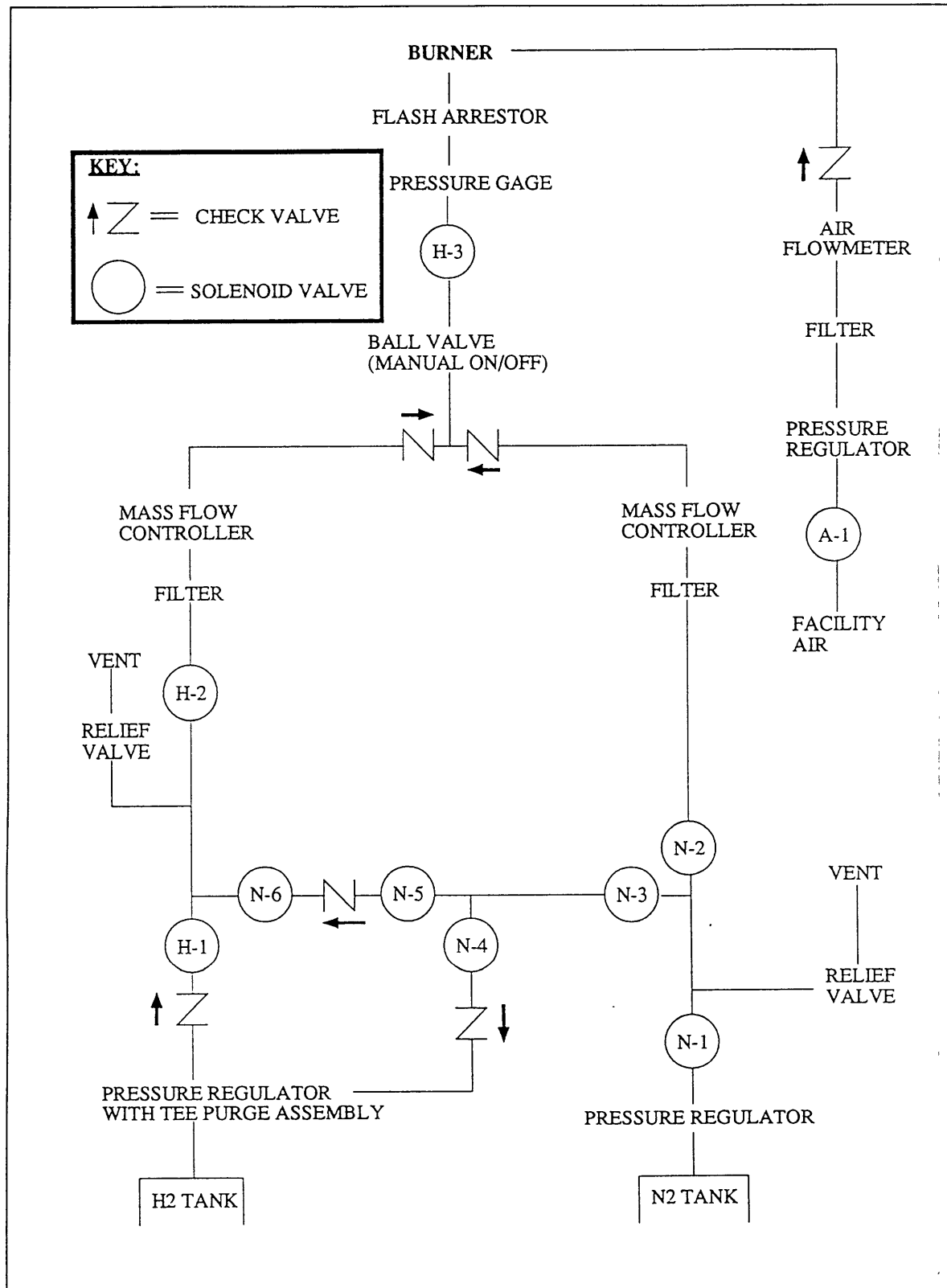


FIGURE 2.2 : FLOW CONTROL DIAGRAM (ADAPTED FROM [16])

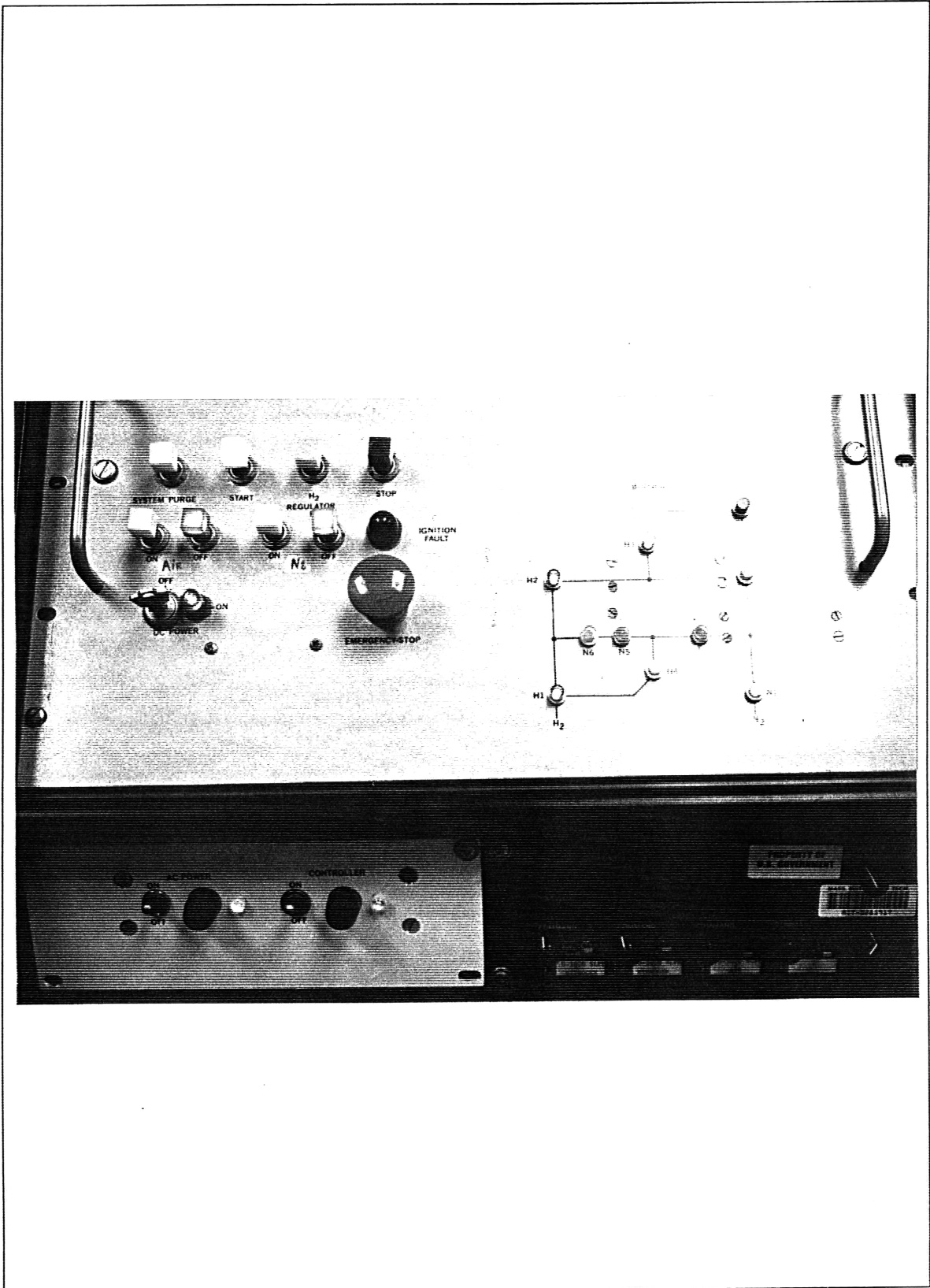


FIGURE 2.3 : FACILITY CONTROL PANEL

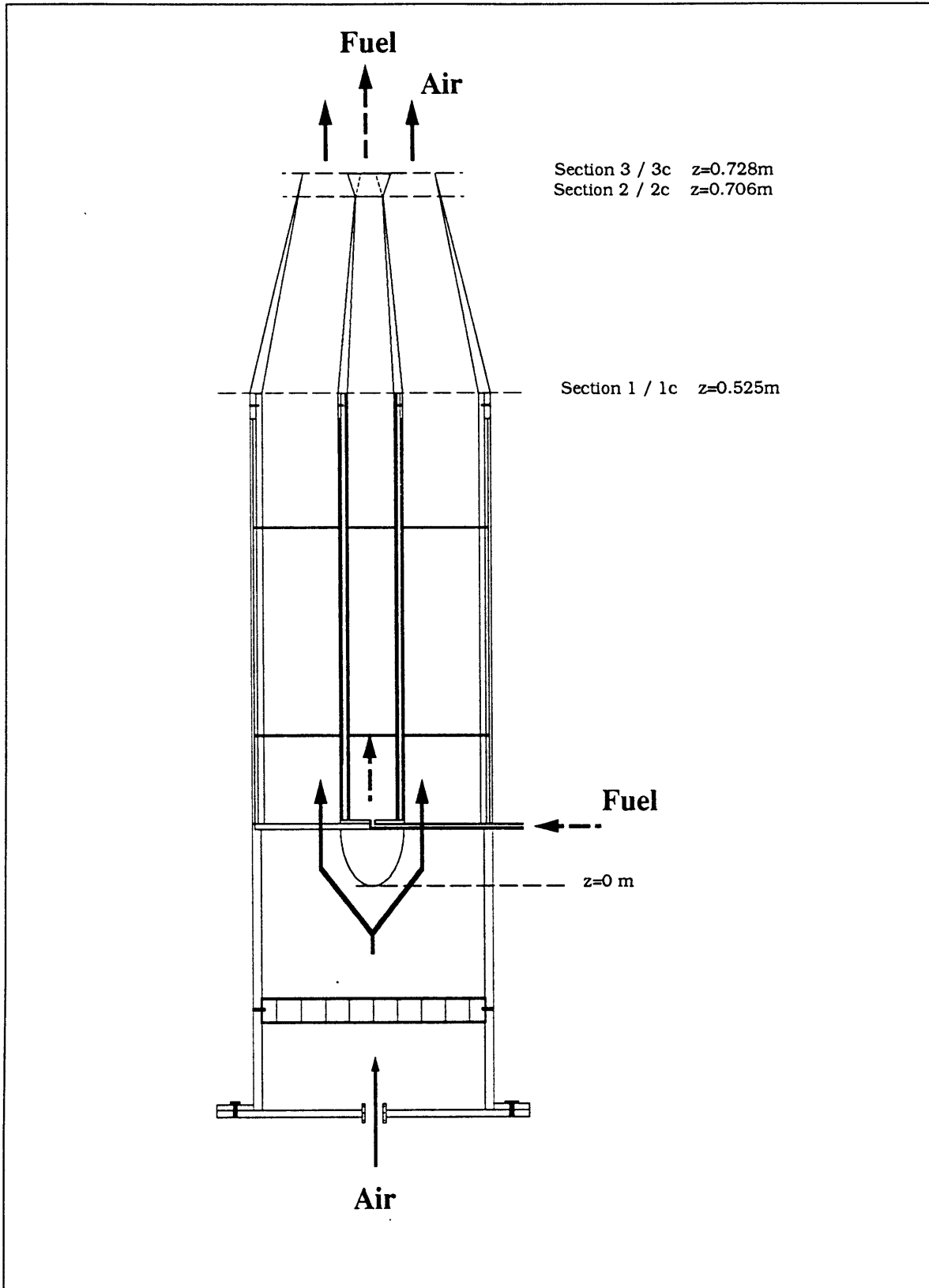


FIGURE 2.4 : ANNULAR BURNER (VERTICAL SECTION)



# 3. Lobed nozzle design

The design of the lobed mixer nozzle used for the study of the mixing enhancement associated with lobed mixers in reacting flow is discussed in this chapter. First, as a guideline, the essential processes responsible for the mixing enhancement associated with lobed mixers are introduced. Second, the important factors that determine the design are discussed. These include fluid dynamic issues (e.g. production of streamwise vorticity and boundary layer blockage) and structural issues (thermal stresses). At last, the final design choices are described and justified using the results of the analysis that has been developed.

## 3. 1. Theoretical background

This section discusses the role of the different components of vorticity (streamwise and normal) on the mixing process in a shear layer. In particular, the geometric and flow parameters that are important to the mixing in a lobed mixer are pointed out. This analysis will allow a better understanding of the mixing in a shear layer and will be used as a guideline for the choice of the lobed mixer design parameters.

### 3. 1. 1. Vorticity in a shear layer

In a two-dimensional shear layer (e.g. for a splitter plate geometry), the flow is dominated by normal (spanwise) vorticity [5]. The velocity differential between the two flows results in a Kelvin-Helmholtz instability, which occurs downstream of the trailing

edge. For axisymmetric shear layers, these spanwise vortices take the form of a “ring” vortex roll similar to the one shown for a lobed mixer in Figure 3.1. While these structures provide the basic mechanism for mixing, the introduction of streamwise vorticity into the flow can be used to augment mixing.

Investigating the physics of the production of streamwise vorticity, Werle, *et al.* [33] found that the vortex formation was an inviscid process. The transverse penetration of the lobes into the flow causes the pressure to vary along the lobes in the spanwise direction. Due to this non-uniform loading, streamwise vorticity is shed from the trailing edge (similarly to the generation of streamwise vorticity by a wing of finite span), as shown on Figure 3.2.

In the case of a co-flow of two fluids with different velocities, the shear layer downstream of the trailing edge will consist of streamwise vorticity associated with the transverse dimension of the mixer (lobe penetration) and spanwise vorticity due to the velocity differential between the two flows [2], [8].

### **3. 1. 2. Lobed mixer enhancement**

Lobed mixers increase the mixing rate by introducing streamwise vorticity into the flow. These relatively large-scale streamwise vortices entrain additional fluid into the mixing layer. Thus, the interface between the two streams is augmented by increasing the strength of the shed circulation associated with the streamwise vorticity, as shown in numerical results by Elliot [8], [9]. Thus, the interface between the fluids is stretched and the interfacial area is increased.

Furthermore, lobed mixers also increase the length of the trailing edge, which also accounts for the overall increase in interfacial area. Manning [14] compared the relative importance of this area increase with the importance of the introduction of streamwise vorticity into the flow. He experimentally determined through the comparison between three different mixer geometries that the fraction of mixing augmentation due to the streamwise vorticity (as opposed to the fraction due to the extended trailing edge length) increases from 37% to 64% as the velocity ratio between the two streams increases from 1.0 to 2.0. The three geometries he studied were a flat “splitter” plate (as a “baseline” for



comparison), a convoluted plate (which convolutes the shear layer in the same way as the lobed mixer but introduces no streamwise vorticity) and a lobed mixer.

These results were confirmed by experiments on axisymmetric lobed mixers by Samimy, *et al.* [4]. In addition, the fraction of mixing enhancement due to streamwise vorticity was also found by Samimy to increase with downstream distance.

The spanwise vorticity is set by the velocity difference between the two streams. The spanwise circulation scales approximately (Barber, [2]) as :

$$\Gamma_{sp} \propto \frac{r-1}{r+1}, \quad (3.1)$$

where  $r$  is the velocity ratio between the two flows.

The streamwise circulation, evaluated on a path encircling half a lobe in the plane of the trailing edge, scales approximately (Barber, [2]) as :

$$\Gamma_{st} \propto U_{mean} \mathcal{H} \tan \alpha, \quad (3.2)$$

where  $\alpha$  is the lobe ramp angle (i.e. the angle between the lobes and the free stream velocity) and  $\mathcal{H}$  is the lobe height. Therefore,  $\mathcal{H}$  and  $U_{mean}$  being fixed, one can write :

$$\Gamma_{st} \propto \tan \alpha \quad (3.3)$$

The most important parameters influencing the mixing in a lobed mixer are the lobe penetration (ramp angle) and the velocity ratio between the two co-flowing streams.

## 3. 2. Preliminary design considerations

The design of the mixer nozzle will now be discussed. Since this design uses extensively the overall design performed by McGrath [16], the most important results of the earlier design are reviewed. These include most notably the shape of the burner, the variations of the cross-sectional area along the burner, the pressure gradient across the nozzle in both the core and the co-flow, and the geometry of the non-lobed nozzle.

Once these preliminary remarks are made, the details of the lobed mixer are discussed. The design is based on recommendations made by McGrath, as well as on geometric

features used in recent lobed mixer designs (Waitz and Underwood [32], Samimy, *et al.* [4]). The preliminary design choices included :

- the choice of a 6-lobe mixer, which was a trade-off between the amount of streamwise vorticity introduced into the flow and the scale of the structures in the shear layer (more lobes would mean smaller lobes and thus smaller structures, which might create resolution problems for the measurements to be taken in the shear layer downstream of the mixer),
- ramp angles were chosen between  $10^\circ$  and  $30^\circ$  (to introduce as much streamwise vorticity as possible into the flow without creating separation problems),
- the core flow cross-sectional exit area was chosen to match as closely as possible the value for the non-lobed mixer, to yield the same range of velocity ratios in both lobed and non-lobed mixers,
- the metal was chosen to be stainless steel 316 mainly because of its heat resistance and mechanical strength.

### 3. 2. 1. a. Fuel composition

The composition of the hydrogen-nitrogen mixture used as the fuel is an important parameter for the design, since it influences directly the viscosity and the density of the core flow. Hence, parameters such as the Reynolds number, the boundary layer thickness or the heat transfer to the nozzle, among others, depend upon the composition of the mixture.

The composition chosen as a baseline for performing the design trades must yield conservative estimates for each design constraint. Thus, the composition which yields the thickest boundary layer and the one that yields the highest heat transfer to the metal of the nozzle (for thermal stress considerations) must be determined.

In the following sections, the design analysis are conducted using an “equivalent fuel”. The assumption that both hydrogen and nitrogen behave like ideal gases is made. Under this assumption, the equivalent density and viscosity of the mixture (designated as “fuel” from now on) are :

$$\rho_{fuel} = x \cdot \rho_{H_2} + y \cdot \rho_{N_2} , \quad (3.4)$$

$$\mu_{fuel} = x \cdot \mu_{H_2} + y \cdot \mu_{N_2} , \quad (3.5)$$

where  $x$  and  $y$  are the mass fractions of  $H_2$  and  $N_2$  in the mixture. Using this assumption, the design fuel composition is determined and used for the calculation of the design constraints.

### 3. 2. 1. b. Geometry of the “baseline” configuration

Most of the dimensions of the burner were chosen by McGrath [16], and were not modified. In particular, the “baseline” (non-lobed) core nozzle was kept as it was (a vertical section of the burner is shown on Figure 2.4). The dimensions of this nozzle are shown on Figure 3.3. The dimensions of the co-flow nozzle are given on Figure 3.4.

The lobed and the non-lobed nozzles were tested under the same upstream conditions to compare the downstream flow patterns shed by each geometry. Therefore, those two geometries were chosen to be as similar as possible, but for the presence or absence of lobes.

The co-flow and the “baseline” (non-lobed) nozzle have been designed to apply a favorable pressure gradient upon the flow, in order to avoid flow separation. Thus, the inner diameter of each section of the burner (co-flow and core-flow) decreases towards the exit of the nozzles :

$$\text{for the core flow } \begin{cases} A_{1c} = 1.95 \times 10^{-3} m^2 \\ A_{3c} = 5.07 \times 10^{-4} m^2 \end{cases}, \text{ and for the co flow, } \begin{cases} A_1 = 3.72 \times 10^{-2} m^2 \\ A_3 = 1.48 \times 10^{-2} m^2 \end{cases}.$$

Using Bernouilli’s equation, one can calculate the corresponding pressure gradient. For the co-flow :

$$\frac{P_3}{\rho_{air}} + \frac{v_3^2}{2} + gz_3 = \frac{P_1}{\rho_{air}} + \frac{v_1^2}{2} + gz_1. \quad (3.6)$$

Conservation of the mass yields :

$$\rho_3 v_3 A_3 = \rho_1 v_1 A_1 , \quad (3.7)$$

Assuming the gases are incompressible (which is a valid approximation since the maximum Mach number reached in the burner is of the order of  $M = 0.04$ ), equation (3.7) gives :

$$v_3 A_3 = v_1 A_1. \quad (3.8)$$

Substituting in equation (3.6) yields :

$$\Delta P = \rho_{air} \left[ \frac{v_1^2}{2} \left( 1 - \left( \frac{A_1}{A_3} \right)^2 \right) - g \Delta z \right]. \quad (3.9)$$

Similar equations can be written for the core flow :

$$\Delta P_c = \rho_{fuel} \left[ \frac{v_{1c}^2}{2} \left( 1 - \left( \frac{A_{1c}}{A_{3c}} \right)^2 \right) - g \Delta z \right]. \quad (3.10)$$

The results are :

$$\frac{P_3 - P_1}{P_1} = -1.13 \times 10^{-3} \quad \text{and} \quad \frac{P_{3c} - P_{1c}}{P_{1c}} = -2.47 \times 10^{-4}.$$

Using this “baseline geometry”, a first design of lobed nozzle was chosen. The geometry was then modified step by step to meet all the design requirements. The final design is presented in Section 3. 5.

### 3. 3. Flowfield constraints

The first concern in the design process is to ensure that the lobed nozzle to be fabricated produces the required flow pattern. This section details the analytical methods employed to insure that the designed lobed nozzle generated the required flow patterns.

#### 3. 3. 1. Introduction of streamwise vorticity into the flow

The analysis presented in Section 3.1 shows that increasing the ramp angle increases the production of streamwise vorticity. The upper limit of the ramp angle is given by the occurrence of flow separation along the lobes. According to Tew [27], ramp angles up to

30° are acceptable in most cases. Angles between 15° to 25° are commonly used ([4], [32]). For the present lobed mixer, the ramp angle will also be chosen within this range to avoid separation problems.

In addition, the introduction of streamwise vorticity into the flow is particularly important within the region where the flow leaves the nozzle at an angle equal to the lobe ramp angle (the angle between the lobes and the free stream velocity, see Section 3.1). Hence, to maximize the amount of streamwise vorticity introduced into the flow, one has to maximize the amount of fluid going through the troughs of the lobes, as discussed in the next section.

### **3.3.2. Boundary layer blockage**

For lobed mixer geometries, it has been observed [12] that the boundary layers are pushed to the troughs of the lobes, as shown in Figure 3.5. As the boundary layer thickness increases, low momentum fluid fills the lobes. As indicated in Figure 3.5, this boundary layer blockage reduces the effective ramp angle and lobe height, reducing the amount of streamwise vorticity introduced in the flow, as a consequence of eqn. (3.2).

Krasnodebski, *et al.* [13] have shown that if the boundary layers occupy more than approximately 20% of the lobes cross-sectional area (based on the displacement thickness), the reduction of the amount of streamwise vorticity introduced into the flow is significant.

In the present section, the displacement thickness is determined for each flow (fuel and air), in order to estimate the boundary layer blockage in the lobes.

#### **3.3.2. a. Determination of the design fuel composition**

To determine the dependence of the boundary layer thickness upon the composition of the fluid, one can use Michel's relationship [17], which gives the displacement thickness as a function of the distance from the leading edge in the case of an incompressible turbulent boundary layer over a flat plate (Michel's relationship was preferred to a Blasius flow since it is valid for a larger range of flow configurations). Assuming that the

boundary layer inside the cylindrical burner grows at the same rate as for a flat plate with no pressure gradient, one can write :

$$\delta^* = 0.02208z \text{Re}_z^{-1/6} , \quad (3.11)$$

i.e.

$$\delta^* = 0.02208z \left( \frac{(x \cdot \rho_{H_2} + y \cdot \rho_{N_2}) \nu z}{x \cdot \mu_{H_2} + y \cdot \mu_{N_2}} \right)^{-1/6} . \quad (3.12)$$

Since  $x + y = 1$ , equation (3.12) gives :

$$\delta^* = 0.02208z \left( \frac{(x(\rho_{H_2} - \rho_{N_2}) + \rho_{N_2}) \nu z}{x(\mu_{H_2} - \mu_{N_2}) + \mu_{N_2}} \right)^{-1/6} . \quad (3.13)$$

Under standard conditions, the density and viscosity of  $H_2$  and  $N_2$  are :

$$\begin{cases} \rho_{H_2} = 8.38 \times 10^{-2} \text{ kg} \cdot \text{m}^{-3} \\ \mu_{H_2} = 8.87 \times 10^{-6} \text{ kg} \cdot \text{m}^{-1} \cdot \text{s}^{-1} \end{cases} \quad \text{and} \quad \begin{cases} \rho_{N_2} = 1.165 \text{ kg} \cdot \text{m}^{-3} \\ \mu_{N_2} = 1.76 \times 10^{-5} \text{ kg} \cdot \text{m}^{-1} \cdot \text{s}^{-1} \end{cases}$$

The maximum of the displacement thickness over the range  $x < 0.86$  (cf. Section 2.2.1.a) can thus be calculated. One finds from equation (3.13) that :

$$\delta^* = \delta^*_{\max} \text{ for } x = 0.86 .$$

Therefore, the boundary layer was conservatively estimated assuming the fuel stream contains 86% of  $H_2$  and 14% of  $N_2$ .

### 3. 3. 2. b. Pressure gradient along the nozzle

To isolate the effect of the lobes on the flow from the effect of other differences between the two geometries, the lobed nozzle was designed to match as closely as possible the non-lobed nozzle for the conditions which do not depend upon the presence of the lobes. Thus, the cross-sectional area of the lobed nozzle was designed to match the pressure gradient with the gradient obtained in the case of the non-lobed nozzle. The calculation of the pressure gradients for the lobed nozzle is similar to the one that has been conducted in Section 3.2.1.b for the non-lobed nozzle. For the lobed nozzle, the flow

conditions along the nozzles in each stream (air and fuel) can be divided into 3 sections, depending on the pressure gradient applied upon the flow in each case. These sections are limited by the cross-sections indicated in Figure 2.4.

Using Bernouilli's equation for the present geometry yields :

$$\left\{ \begin{array}{l} \frac{P_2 - P_1}{P_1} = -8.48 \times 10^{-4} \\ \frac{P_3 - P_2}{P_2} = -2.86 \times 10^{-4} \end{array} \right. \quad \text{and} \quad \left\{ \begin{array}{l} \frac{P_{2c} - P_{1c}}{P_{1c}} = -1.78 \times 10^{-4} \\ \frac{P_{3c} - P_{2c}}{P_{2c}} = -6.91 \times 10^{-5} \end{array} \right. .$$

As mentioned previously, these pressure gradients are favorable and will therefore reduce the thickness of the boundary layer and reduce the risks of separation for both the core and the co flow. The overall pressure gradients across the lobed nozzle are the same as those for the non-lobed nozzle.

### 3. 3. 2. c. Displacement thickness

This section outlines the method, described in Schlichting [24] (pp. 673-686), which was used to determine the boundary layer thickness at the exit of the nozzle. The analysis presented hereafter was applied to calculate the growth of the boundary layer from section 1 and 1c to sections 2 and 2c (cf. Figure 2.4). The calculation was iterated for each step of the design, until the chosen geometry yielded an acceptable value for the boundary layer blockage. Because of the lobes, the boundary layer growth across the lobed part of the nozzle can not be determined by this method, and was estimated using empirical results by Krasnodebski [12].

To describe the behaviour of a boundary layer, it is necessary to know its thickness and to have an indication of the velocity distribution. The boundary layer thickness is commonly characterized by the displacement thickness ( $\delta^*(z)$ ), the momentum thickness ( $\delta_2(z)$ ) and the energy thickness ( $\delta_3(z)$ ), where  $z$  designates the axial coordinate along the cylinder separating the core flow and the co flow.

These quantities can be non-dimensionalized by introducing appropriate Reynolds numbers :

$$R_2 = \frac{\delta_2 U}{\nu} \quad \text{and} \quad R_3 = \frac{\delta_3 U}{\nu}. \quad (3.14.a, b)$$

The velocity profile depends on the external pressure gradient, and can be characterized by a number of *shape factors*. Traditionally, the following dimensionless factors are used :

$$H_{12} = \frac{\delta_1}{\delta_2}, \quad H_{23} = \frac{\delta_2}{\delta_3} \quad \text{and} \quad H_{32} = \frac{\delta_3}{\delta_2}. \quad (3.15.a, b, c)$$

Measurements indicate that turbulent velocity profiles can be described approximately by a one-parameter family of curves. Based on that observation, Truckenbrodt [30] introduced a *modified shape factor* H :

$$H = \exp \left[ - \int_{(H_{23})_{\infty}}^{H_{23}} \frac{dH_{23}}{(H_{12} - 1)H_{23}} \right]. \quad (3.16)$$

According to Wieghardt [34],  $H_{12}$  and  $H_{23}$  can be related through the equation (3.17) :

$$H_{12} = \frac{H_{32}}{3H_{32} - 4}. \quad (3.17)$$

Combining equation (3.16) and equation (3.17) yields :

$$H = 0.5442 H_{23} \left( \frac{H_{23}}{H_{23} - 0.5049} \right)^{1/2}. \quad (3.18)$$

Therefore, once H and  $R_3$  are determined, one can find the values of  $H_{12}$ ,  $H_{23}$ ,  $\theta$  and  $\delta^*$ , fully characterizing the behaviour of the boundary layer.

Truckenbrodt [29], [30] worked out an approximate method to determine both H and  $R_3$  by integrating the equations of the turbulent boundary layer. This method is valid for two-dimensional as well as axially symmetric flows and yields :

$$R_3(z) = \left( \frac{1}{\nu'} \frac{E_3(z_1) + \int_{z_1}^z U^{3+2b} dz}{[U(z)]^{2(1+b)}} \right)^{1/(1+b)} \quad (3.19)$$



with

$$E_3(z_1) = v' \left\{ [U(z_1)]^2 \cdot R_3(z_1) \right\}^{1+b}, \quad (3.20)$$

where  $v' = 80v$  and  $b=0.152$ .

The external free-stream velocity  $U(z)$  is found from the potential theory, and the variation of  $R_3$  between two cross sections can be calculated.

Transforming the boundary layer equations, Truckenbrodt shows that  $H(z)$  can be written as follows :

$$H(z) = U(z)G(z) \cdot [N(z)]^{-1/c}, \quad (3.21)$$

with

$$G(z) = G(z_1) + \int_{z_1}^z U^{2(1+b)} dz \quad (3.22)$$

and

$$N(z) = N(z_1) + c \int_{z_1}^z U^{2(1+b)+c} G^{c-1} dz, \quad (3.23)$$

where  $n=3+2b$  and  $c=4.0$ . The initial values are :

$$\begin{cases} G(z_1) = v' \left\{ H(z_1) \cdot [U(z_1)]^{1+2b} [R_3(z_1)]^{1+b} \right\} \\ N(z_1) = \left[ \frac{U(z_1) \cdot G(z_1)}{H(z_1)} \right]^c \end{cases} \quad (3.24.a, b)$$

Once the values of  $R_3$  and  $H$  are known for the cross-sections 1 and 1c of the axisymmetric burner, one will be able to deduce the values for the sections 2 and 2c. The free-stream velocity was assumed to vary linearly across the nozzle, since the cross-sectional areas decrease linearly :  $U(z) \propto z$ .

For the calculation of  $H$  and  $R_3$  in the sections 1 and 1c, the assumption that the turbulent boundary layer starts at  $z=0$  (inlet of the burner) without a laminar inlet

portion is made. This is a valid assumption since the flow exiting the tubing is turbulent. With the assumption that  $U(z) \propto z$ , equations (3.19) to (3.24) yield (Schlichting, [24]) :

$$R_3(z_1) = \left( \frac{\bar{\beta} U z_1}{r v} \right)^{\frac{1}{1+b}}, \quad (3.25)$$

and

$$H(z_1) = \left( \frac{r}{s} \right)^{\frac{1}{c}} = \text{const}, \quad (3.26)$$

with  $\bar{\beta} = 0.0127$  ;  $r = 1+(3+2b)$  and  $s = 1+2(1+b)$ .

Now that  $H(z=z_1)$ ,  $H(z=z_{1c})$ ,  $R_3(z=z_1)$  and  $R_3(z=z_{1c})$  are known, the boundary layer thickness can be calculated for the sections 2 and 2c.

The lobed geometry causes the boundary layer between sections 2 and 3 (and 2c - 3c) to grow even though a favorable external pressure gradient is applied on the flow. According to Krasnodebski [12], considering that the momentum thickness increases by a factor 3 is a conservative estimate of the boundary layer growth across the lobes. The results are outlined in Table 3.1. Detailed results including the values of  $R_3$ ,  $H$ ,  $H_{12}$ , and  $H_{23}$  are given in Appendix B.

	Co Flow (Air)			Core Flow (H <sub>2</sub> + N <sub>2</sub> )		
	Section 1	Section 2	Section 3	Section 1c	Section 2c	Section 3c
Cross-sectional area (m <sup>2</sup> )	1.67×10 <sup>-2</sup>	3.72×10 <sup>-2</sup>	1.48×10 <sup>-2</sup>	1.95×10 <sup>-3</sup>	5.91×10 <sup>-4</sup>	5.07×10 <sup>-4</sup>
Velocity (m.s <sup>-1</sup> )	5.97	13.30	15.00	3.90	12.86	15.00
z (height, in m)	0.525	0.706	0.728	0.525	0.706	0.728
Displacement thickness (m)	1.68×10 <sup>-3</sup>	2.85×10 <sup>-4</sup>	8.55×10 <sup>-3</sup>	2.05×10 <sup>-3</sup>	2.19×10 <sup>-4</sup>	6.57×10 <sup>-4</sup>

TABLE 3.1 : BOUNDARY LAYER GROWTH ACROSS THE NOZZLE

Using this estimate for the displacement thickness, one can determine the boundary layer blockage at the exit section of the lobed mixer. The boundary layers are pushed to

the lobe troughs. Based on the final geometry (cf. Section 3. 5) , in which the lobes are 0.67" long and 0.17" wide, the conservative results shown in Table 3.1 indicate, according to Krasnodebski [12], that the boundary layers occupy less than 5% of the cross-sectional area of the lobes. This value is thus well within the acceptable limit, which is roughly 20%.

### 3. 3. 3. Flame holding

The trailing edge of the lobed mixer must be thick enough to allow the flame to stabilize. On the other hand, the trailing edge should be as thin as possible to minimize the effect of the wake on the shear layer.

Becker and Liang [3] stabilized a hydrogen-air flame on a 0.030" trailing edge thickness for a flow velocity of 82 m.s<sup>-1</sup>. Waitz and Underwood [32] stabilized a hydrogen-air flame on a 0.040" trailing edge thickness for flow velocities of approximately 85 m.s<sup>-1</sup>.

Since the maximum flow velocity reached in the present facility is  $v_3 = 15$  m.s<sup>-1</sup>, the trailing edge thickness of the lobed mixer to be designed could be chosen to be as small as 0.010". Nevertheless, due to mechanical and fabrication constraints, the nozzle trailing edge thickness was chosen to be 0.020". Since the chosen lobe height is  $\mathcal{H} = 0.67$ ", this gives :

$$\frac{\varepsilon}{\mathcal{H}} = 3.0 \times 10^{-2}$$

## 3. 4. Structural constraints : thermal stresses

Another design concern is the impact of the thermal stresses on the lobed nozzle. The stresses were estimated and compared to the elastic limit of the material (stainless steel 316, cf. Section 3. 2).

The first step of the calculation was to determine the temperature profile in the metal. Then, using this temperature profile, the thermal stresses were estimated to provide a conservative estimate for the maximum stress reached within the lobes.

Due to the temperature rise, each wall of the lobes will expand radially and axially. In the axial direction, the material is not constrained and can therefore expand freely. Hence, no thermal stresses will build up axially. In the radial direction, the inside half of each wall will tend to expand towards the inside of the nozzle, while the outside half of the wall will tend to expand towards the outside (cf. Figure 3.6). This will create internal stresses within the lobe walls. Thus, the analysis was conducted for the lobe walls.

Throughout the analysis conservative assumptions are made. The main assumptions are:

- the lobe walls were considered as flat plates since they are planar and their thickness is small compared to their radial and axial dimensions,
- the thickness of the lobes was taken to be constant and equal to the trailing edge thickness. This assumption is conservative since the actual thickness increases away from the trailing edge. Hence, heat will be carried out more efficiently away from the critical zone which is the trailing edge thickness, and the increased thickness will increase the resistance of the nozzle,
- once the temperature gradient across the nozzle was estimated, the temperature profile in the metal was assumed to be linear. This assumption is conservative since the actual profile is convex (cf. Section 3.4.1.a). Therefore, the temperature in each point of the lobes is conservatively estimated, as shown on Figure 3.9.

#### 3. 4. 1. a. Temperature profile in the metal

The heat transfer to a flat plate can be modeled as shown on Figure 3.7. For this situation, the Biot number is [18] :

$$Bi = \frac{2h\varepsilon}{k_{metal}}, \quad (3.27)$$

with

$$h(z) = \frac{k_{fluid}}{z} Nu_z, \quad (3.28)$$

where  $k_{fluid}$  is the thermal conductivity of the fluid on each side,  $Nu_z$  is the Nusselt number based upon  $z$  and  $\varepsilon$  is half the trailing edge thickness.

$Nu_z$  can be estimated for a turbulent boundary layer using empirical correlations [29]. The Biot number is higher in the fuel than in the air. The maximum Biot number over the range of fuel compositions is reached for a fluid composed of 50%  $N_2$  - 50%  $H_2$ . Assuming that the thickness of the metal is constant and equal to the trailing edge thickness ( $2\epsilon = 0.02''$ , where  $\epsilon$  is equal to the half thickness of the lobes), one finds that :

$$Bi_{max} = Bi_{air} \cong 2.2 \times 10^{-3} \ll \frac{1}{4}$$

Hence, as stated by Taine [25], the characteristic time of the conduction through the metal is much smaller than the characteristic time of the convection across the metal-fluid interface. This means that one can consider the temperature to be constant across the thickness of the metal, and no significant thermal stress will build across the thickness of the lobes.

In addition, since the flame is holding along the entire trailing edge of the mixer, one can consider the temperature profile to be quasi one-dimensional :

$$T = T(z). \quad (3.29)$$

The present configuration is similar to the classic problem of a one-dimensional fin [18]. Nevertheless, the fluid is here different for each side of the lobe wall, and the boundary conditions at the edges differ slightly from those of a classical fin calculation.

Since the lobe receives heat through its trailing edge and dissipates heat through its side surfaces, a conservative estimate of the temperature rise in the metal is to consider that both sides of the lobes are immersed in the same fluid yielding the lowest heat transfer coefficient.

At the trailing edge of the lobe, in the recirculation zone, the velocity of the fluid is small. Thus, the heat transfer to the lobe occurs by natural convection. Fischenden and Saunders (in [29]) found that in the case of a flat plate heated by natural convection from its upper surface :

$$Nu_\epsilon = 0.14 \times Ra_\epsilon^{1/3}, \quad (3.30)$$

and :

$$h_{natural} = \frac{0.14k}{\varepsilon} Ra_e^{1/5}. \quad (3.31)$$

The maximum possible  $h_{natural}$  was determined by varying the nature and composition of the gas surrounding the trailing edge within the range determined for the present facility.

Assuming the heat transfer through the trailing edge occurs by forced convection, one can write :

$$h_{forced} = \frac{0.0288k}{z} Re_z^{1/5} Pr^{1/5}. \quad (3.32)$$

By varying the composition of the gas used in eqn. (3.32), one finds that forced convection yields a higher heat transfer coefficient than natural convection in all the possible configurations :

$$h_{forced} > h_{natural}.$$

Therefore, assuming that the heat transfer through the trailing edge occurs by forced convection in the same gas as for the sides of the lobe is conservative, and this assumption was made.

The fin equation can now be used to describe the heat transfer along the lobe, but with different boundary conditions at the edges. It is assumed that the metal temperature in section 1 of the burner is constant and equal to 300 K. This is equivalent to assuming that the lower part of the nozzle is a heat sink.

The temperature of the gas is assumed to be 300 K everywhere but in the wake. In the wake, the adiabatic flame temperature of a hydrogen-air flame is assumed :

$$\begin{cases} T_{ext}(z < H) = 300 \text{ K} \\ T_{ext}(z = H) = 2400 \text{ K} \end{cases}.$$

This external temperature field takes into account the fact that the radiation from a hydrogen-air flame is minor ( $\cong 30\%$ ).

The situation is now represented by the following system (corresponding to the model shown on Figure 3.8), consisting of the fin equation and of particular boundary conditions :

$$\frac{d^2T(z)}{dz^2} - \frac{2h}{\epsilon k}(T(z) - T_{ext}(z)) = 0 , \quad (3.33)$$

$$\begin{cases} T(z=0) = T_0 = 300 \text{ K} \\ -k \frac{dT}{dz}(z=H) = h[T(H) - T_{ext}(H)] \end{cases} . \quad (3.34)$$

The resolution of this system gives the temperature profile in the metal :

$$T(z) - T_0 = A.(e^{mz} - e^{-mz}) , \quad (3.35)$$

with

$$A = \frac{2400 - T_0}{(e^{mH} - e^{-mH}) + \frac{\lambda m}{h}(e^{mH} + e^{-mH})} ,$$

and

$$m = \sqrt{\frac{2h}{\epsilon k}} .$$

The nature of the gas (air or fuel ) and the composition (H<sub>2</sub> and N<sub>2</sub> proportions for the fuel) used in the calculation were then varied to obtain the highest possible temperature rise. This will give the maximum thermal stresses.

A fuel composed of 64% of hydrogen and 36% of nitrogen was found to cause the maximum temperature rise (cf. Appendix C), and the calculation of the thermal stresses was conducted assuming this gas composition. The results are shown on Figure 3.9. The maximum temperature in the metal is reached at the trailing edge :

$$T_{\max} = T(z=H) = 349 \text{ K}.$$

The assumption that the temperature varies linearly with z is made for the calculation of the thermal stresses.

### 3. 4. 1. b. Maximum thermal stress

Timoshenko [28] (pp. 207-209) gives an estimate for the thermal stresses which build up for a flat plate on which a non-constant temperature profile T(z) is applied while held at

the edges. The stress which builds up in the plane of the plate, perpendicularly to the direction along which the temperature varies is :

$$\sigma_y(z) = -\alpha ET(z) + \frac{1}{2H} \int_0^H \alpha ET(\xi) d\xi + \frac{3z}{2H^3} \int_0^H \alpha E \xi \cdot T(\xi) d\xi \quad (3.36)$$

This is a conservative estimate, since the edges of the lobe walls expand some in a practical situation. One finds that the maximum stress is reached at the trailing edge. The result was then compared to the elastic limit of the material (cf. Table 3.2) :

Maximum stress (in psi)	Elastic limit of the material (Stainless 316) (in psi)
2.36×10 <sup>4</sup>	6.0×10 <sup>4</sup>

TABLE 3.2 : MAXIMUM THERMAL STRESS WITHIN THE LOBED MIXER

This estimate is conservative, but shows that the final design choices meet the structural requirements.

### 3. 5. Lobed mixer geometry

The final geometry is shown on Figures 3.10, 3.11 and 3.12. Both the lobed and the non-lobed geometries are presented in Figure 3.13.

The values of the main geometrical parameters were chosen as follows :

- variations of the cross-sectional areas across the nozzle are indicated in Table 3.1,
- ramp angle for the core flow is (cf. Figure 3.10) :  $\alpha_{core} \cong 21^\circ$  ,  
ramp angle for the co flow :  $\alpha_{co} \cong 19^\circ$  ,
- trailing edge thickness :  $\varepsilon = 0.020 \text{ inches}$  .



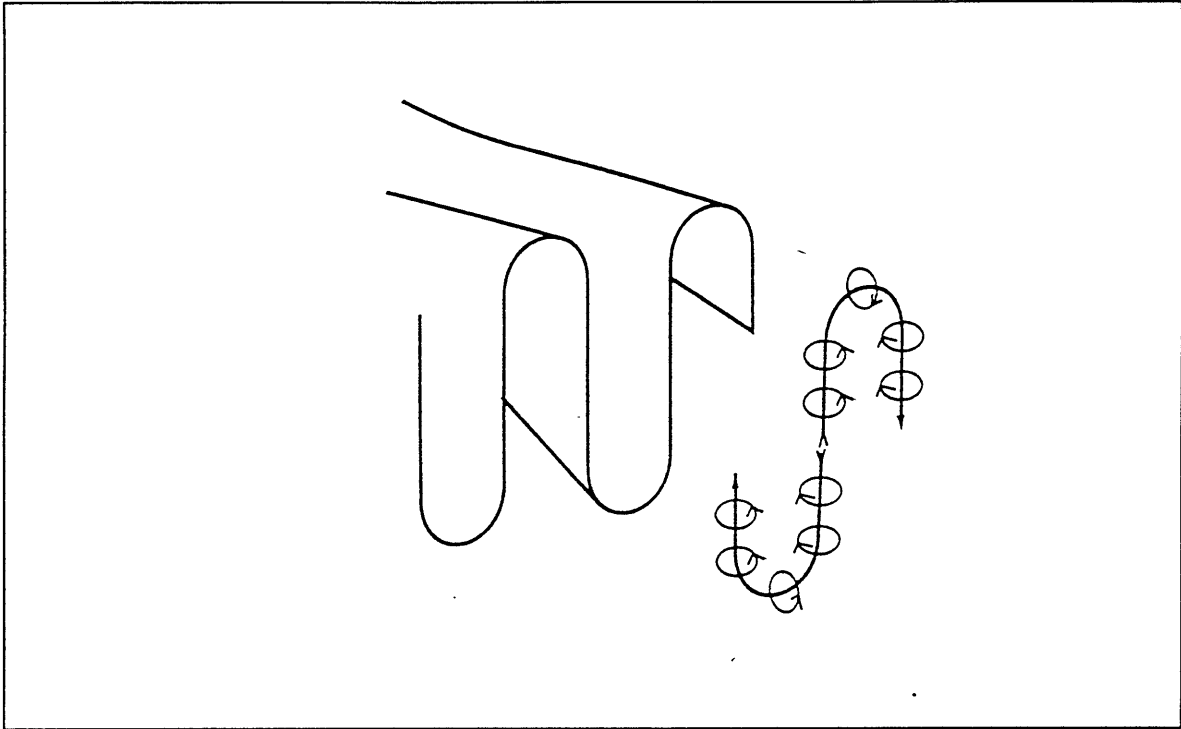


FIGURE 3.1 : SPANWISE VORTICITY ABOUT A LOBED MIXER

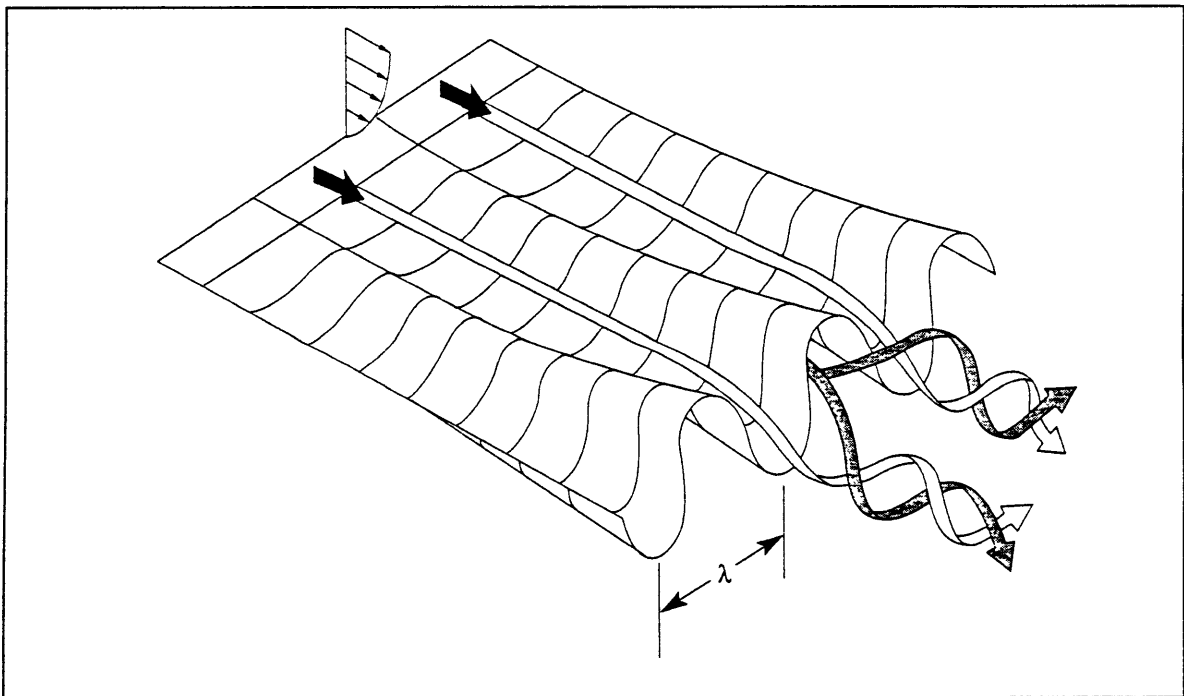


FIGURE 3.2 : FORMATION OF STREAMWISE VORTICITY IN A LOBED MIXER  
(ADAPTED FROM [21])

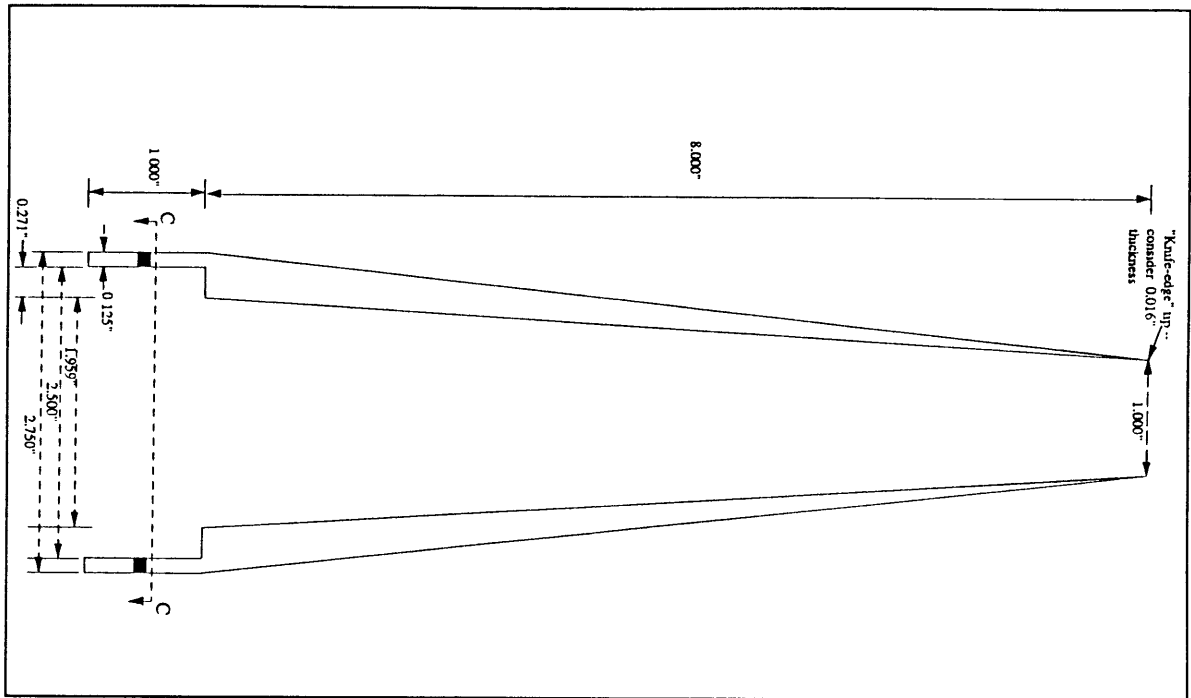


FIGURE 3.3 : DIMENSIONS OF THE NON-LOBED CORE NOZZLE (ADAPTED FROM [16])

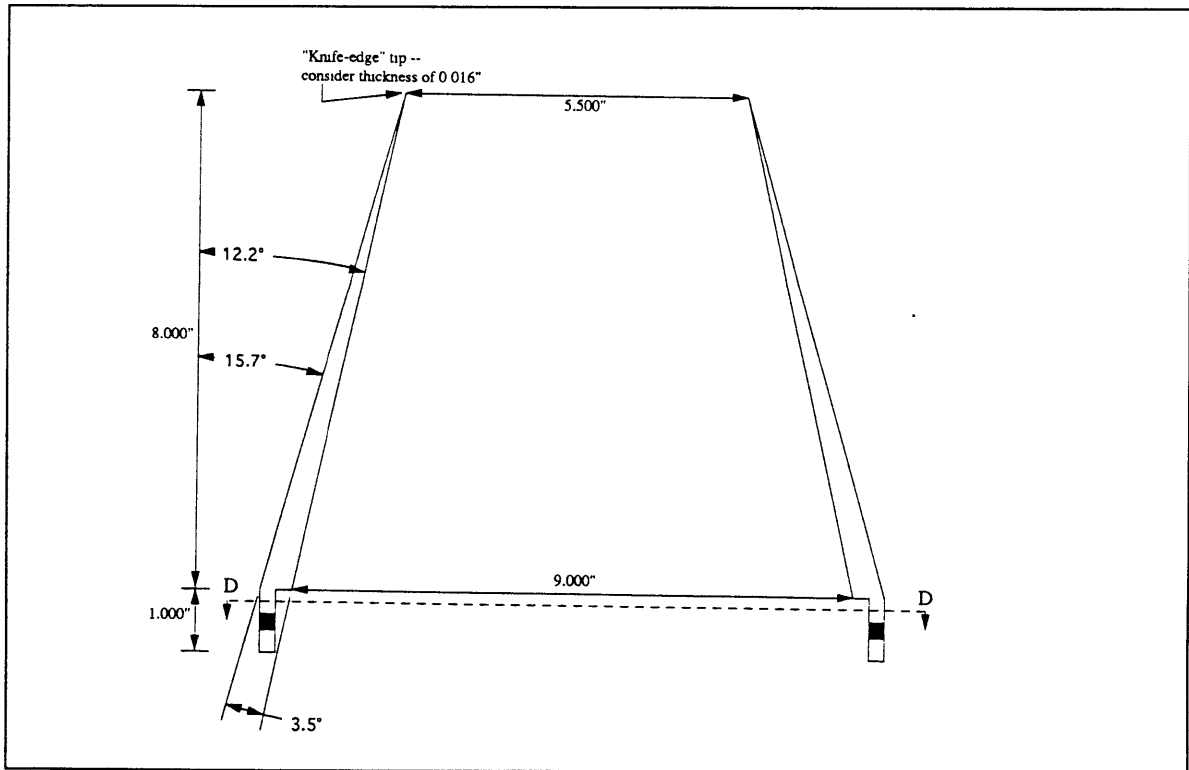


FIGURE 3.4 : DIMENSIONS OF THE CO-FLOW NOZZLE (ADAPTED FROM [16])

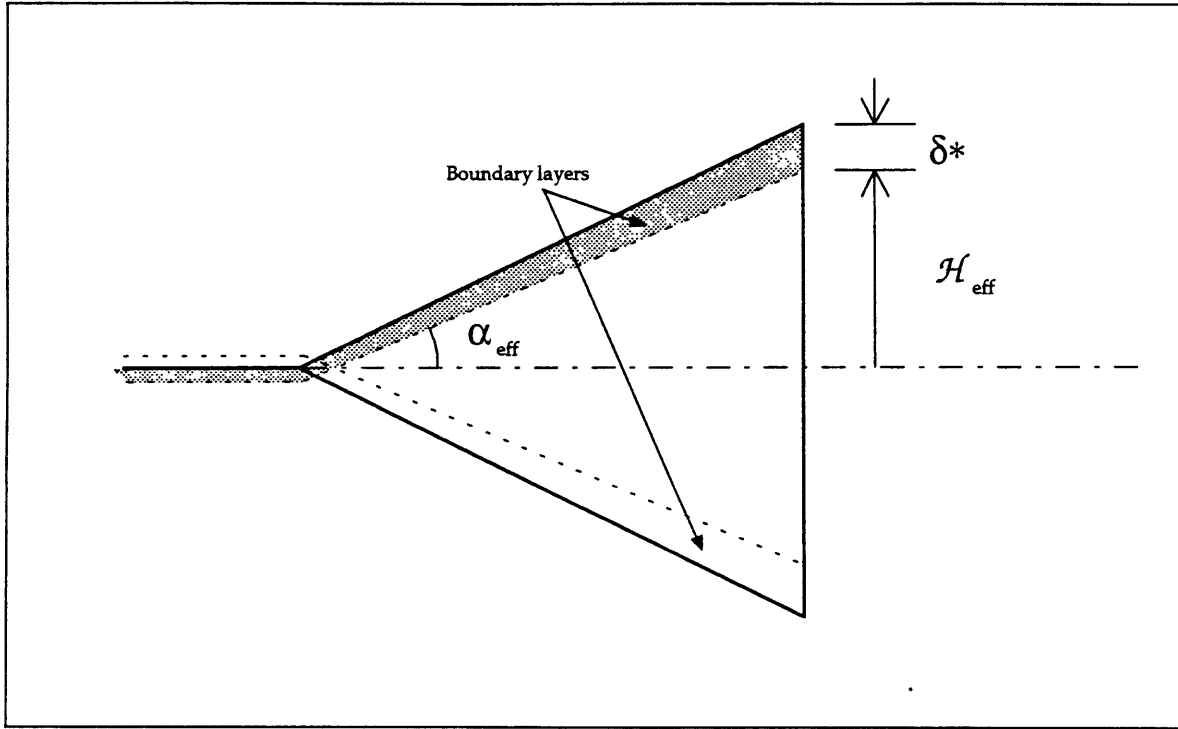


FIGURE 3.5 : BOUNDARY LAYER BLOCKAGE IN A LOBED MIXER

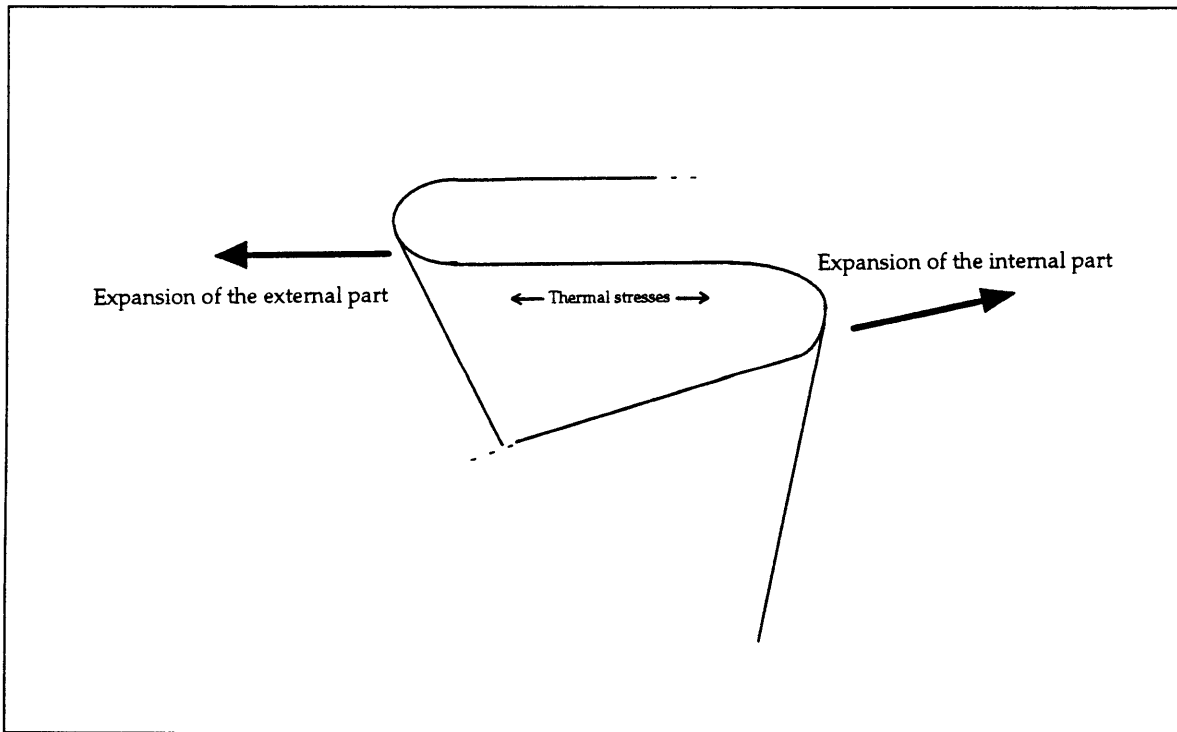


FIGURE 3.6 : THERMAL EXPANSION OF THE LOBE WALLS

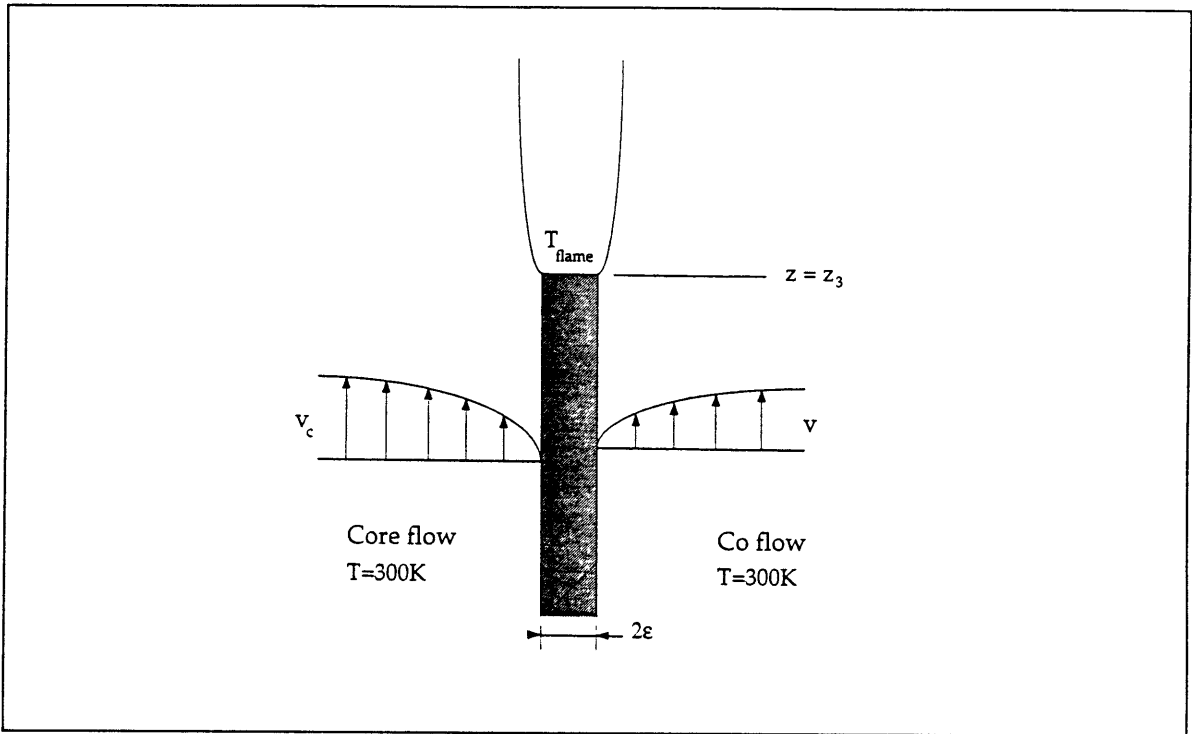


FIGURE 3.7 : HEAT TRANSFER TO A LOBE WALL, PRACTICAL SITUATION

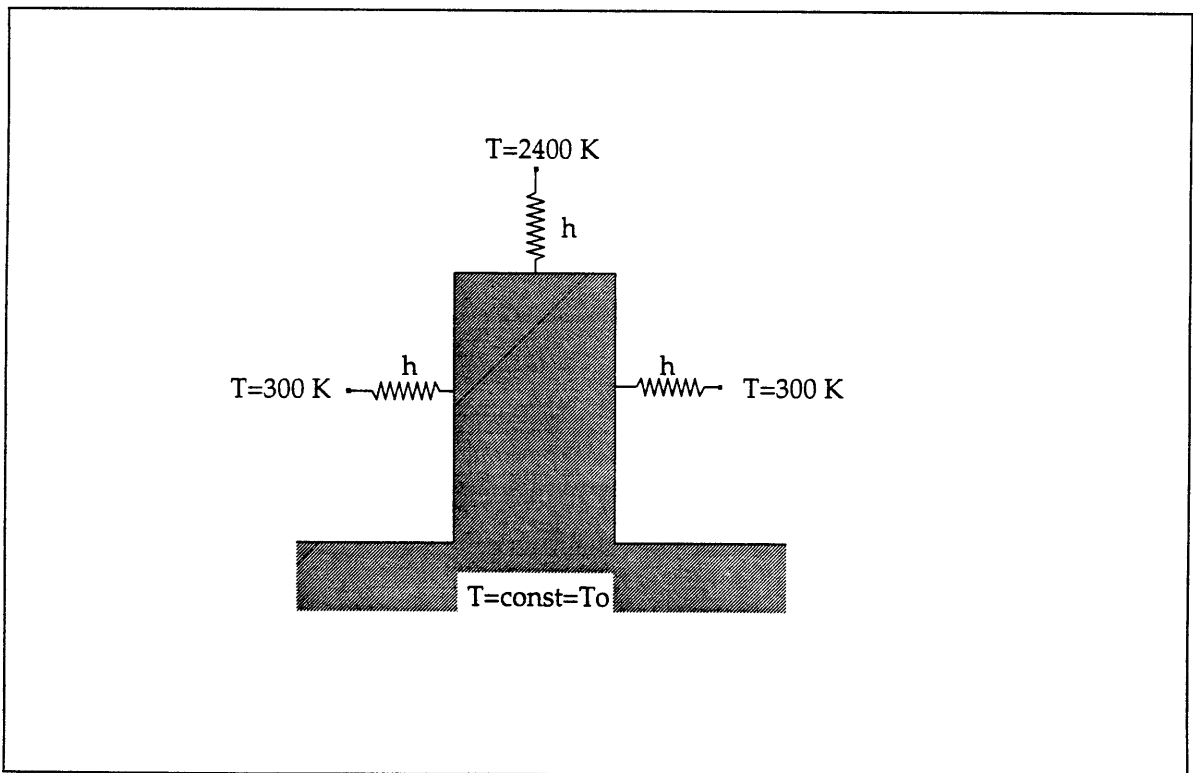


FIGURE 3.8 : MODEL FOR THE HEAT TRANSFER TO A LOBE WALL

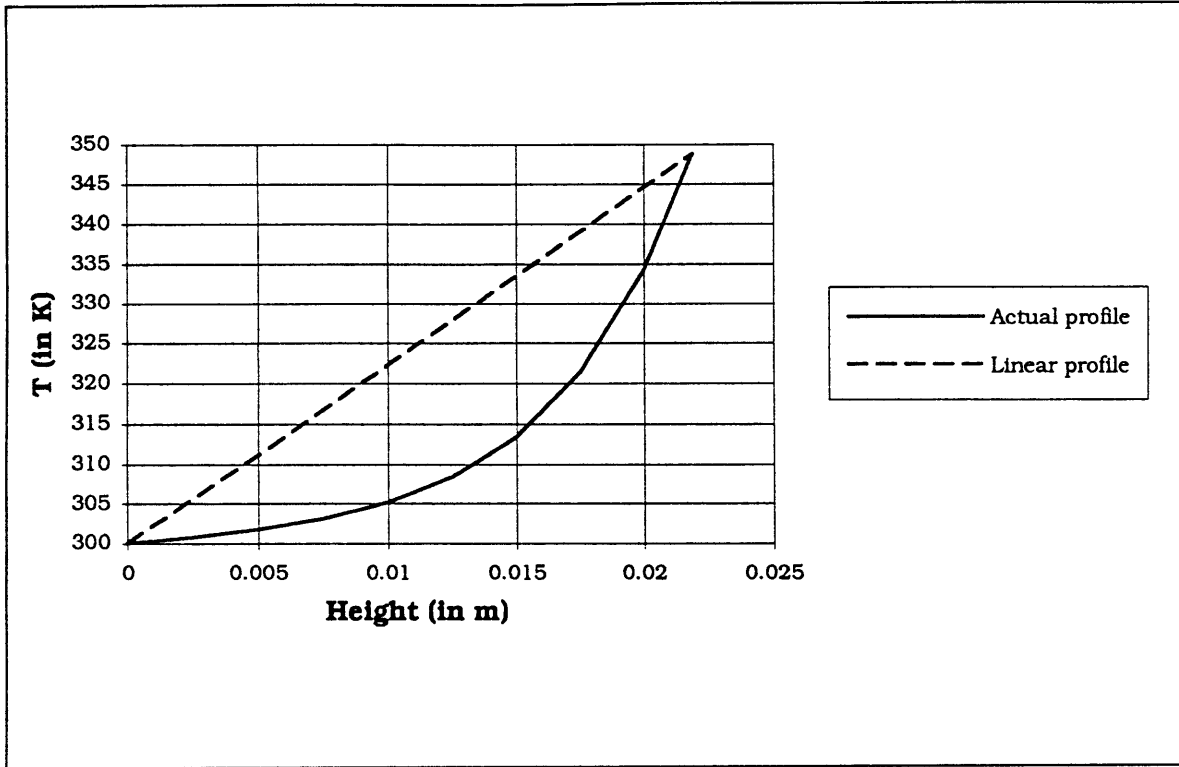


FIGURE 3.9 : TEMPERATURE PROFILE IN THE LOBES ( $Z=0$  AT THE INLET OF THE LOBES)

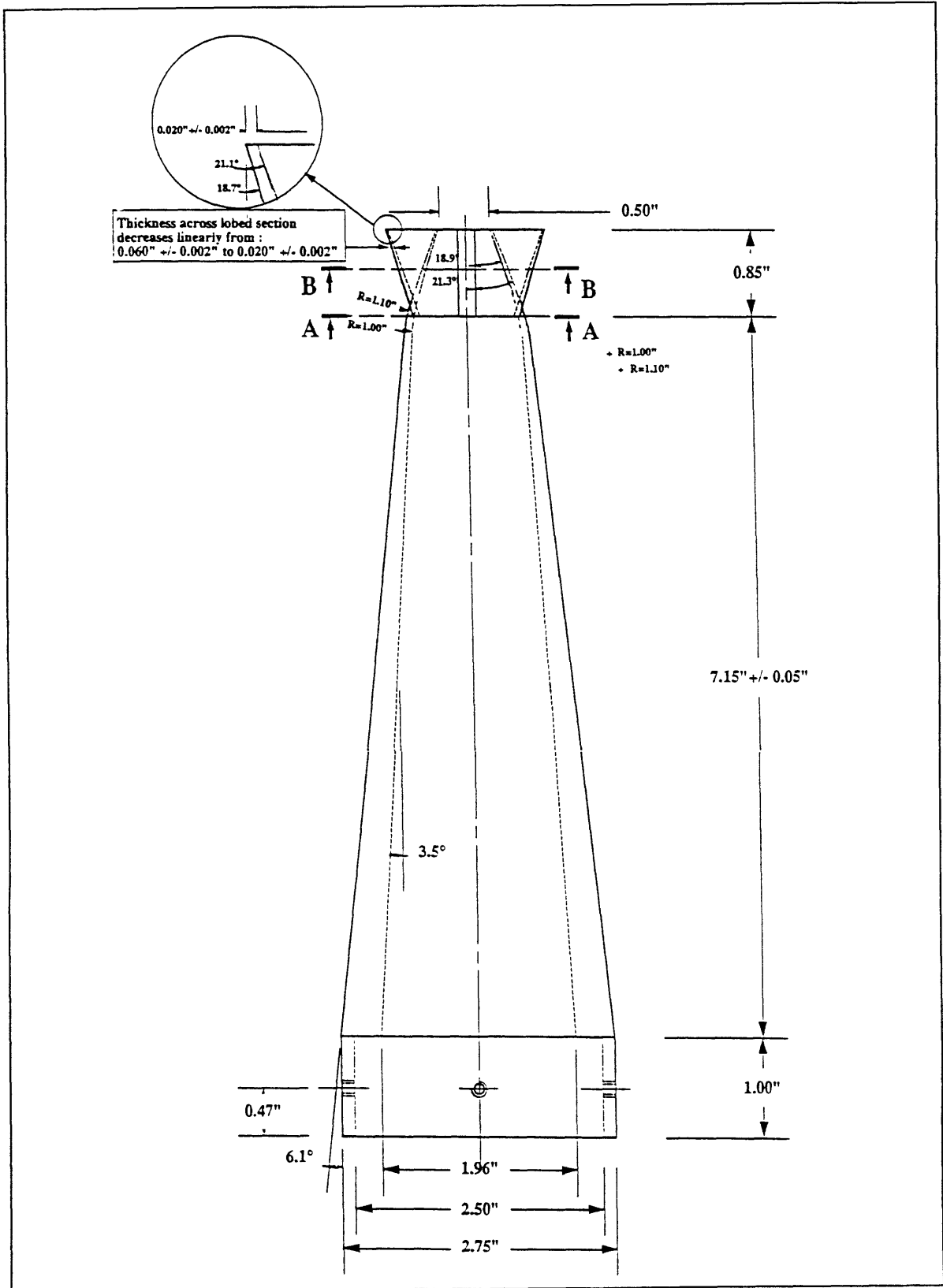


FIGURE 3.10 : LOBED MIXER, FRONT VIEW

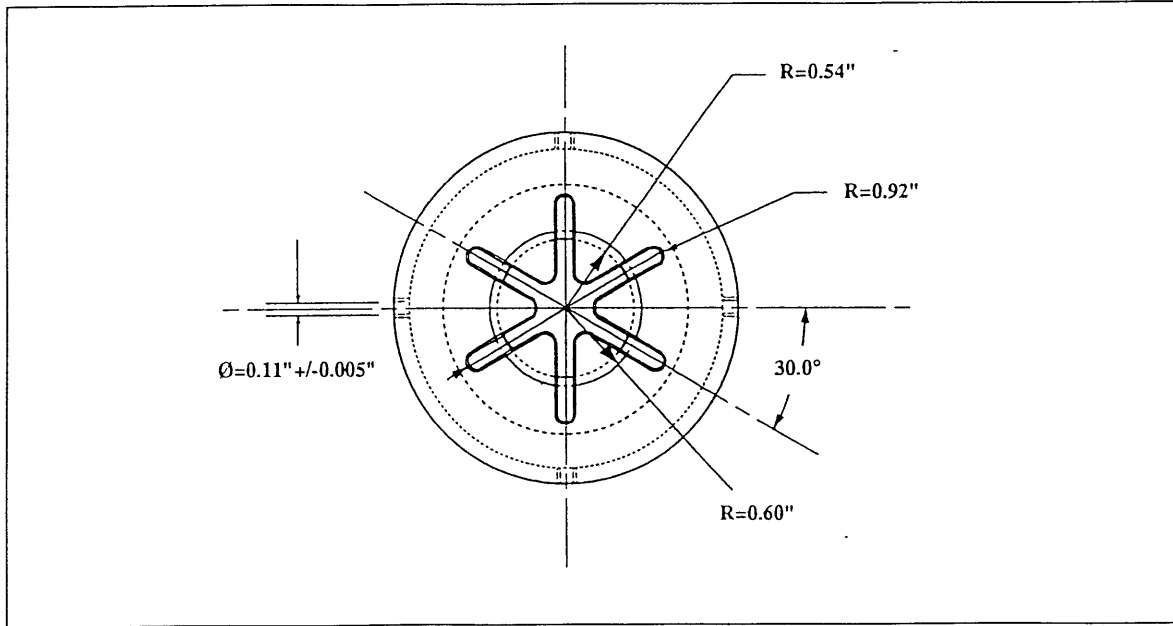


FIGURE 3.11 : LOBED MIXER, UPPER VIEW

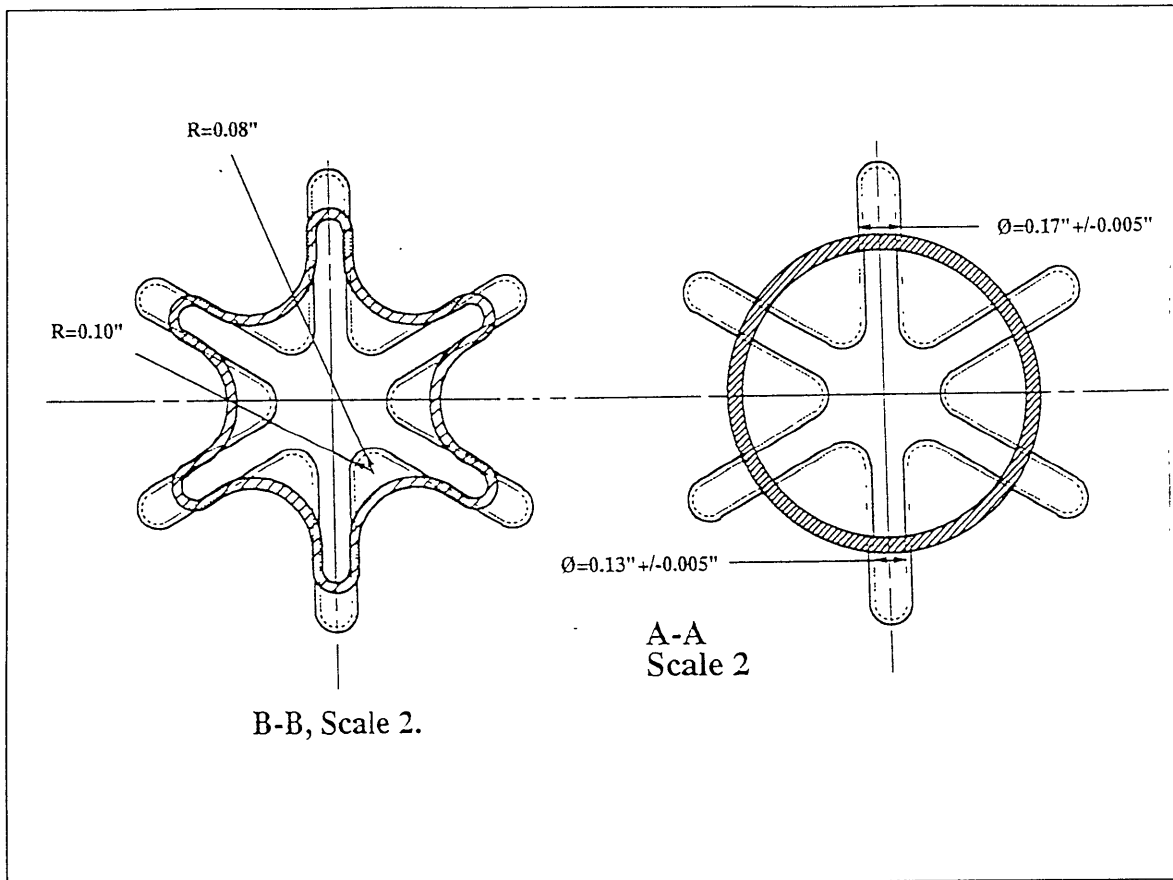


FIGURE 3.12 : LOBED MIXER, CROSS SECTIONS

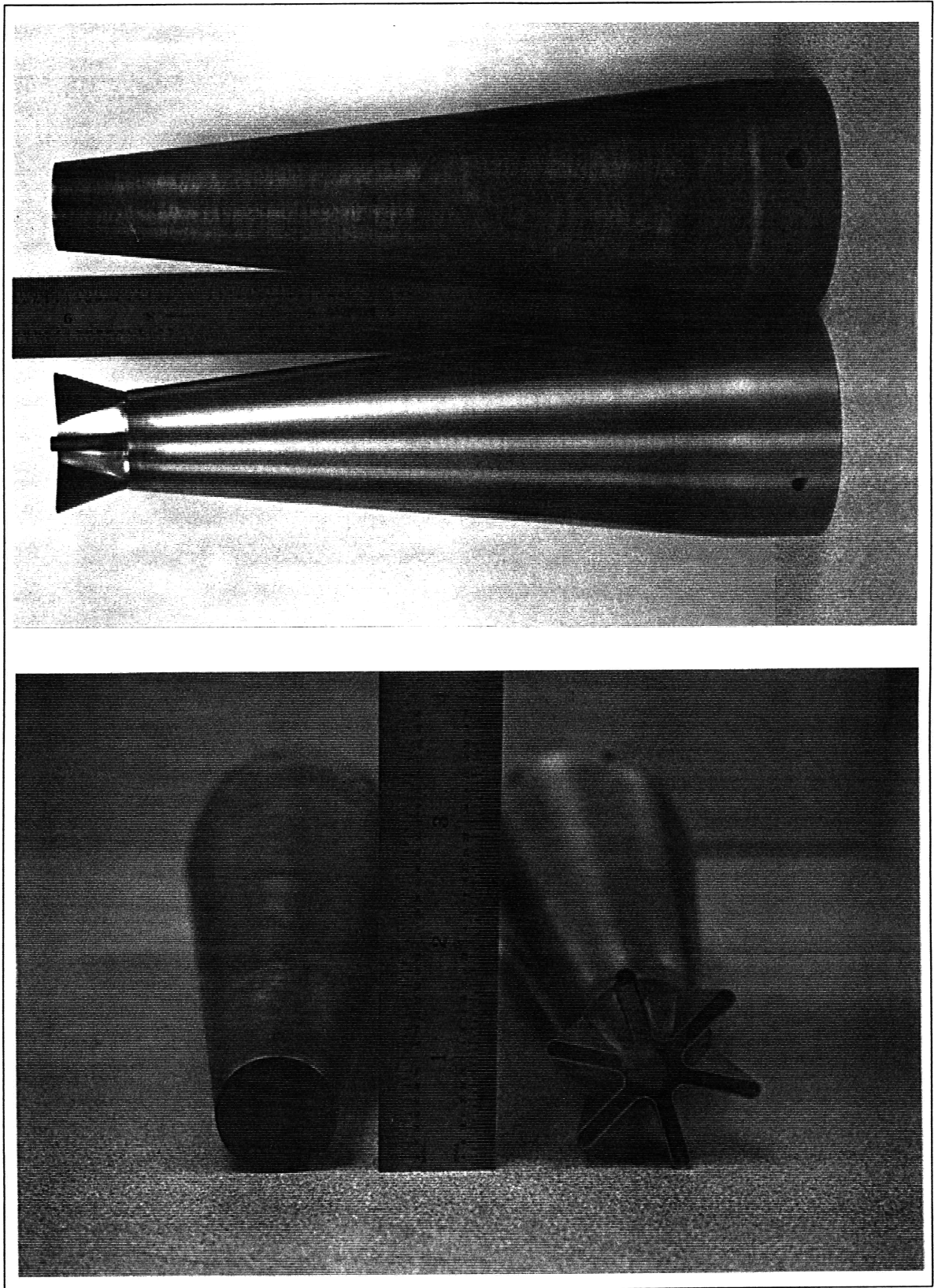


FIGURE 3.13 : LOBED AND NON-LOBED MIXERS



# 4. Experimental approach and results

This section presents and discusses the experiments that were conducted. Initially, the facility was tested for proper functioning, notably to insure maximum safety for the operator. Then, the effective operating range of the facility was investigated. In addition, the flow was visualized using oil flow techniques, to examine the flow field along the lobe walls. Finally, total pressure surveys of the flow fields from both the lobed and the non-lobed mixers were collected to provide a preliminary characterization of the flow field downstream of the lobed mixer.

## 4. 1. Experimental approach

The experiments that were conducted had three main objectives :

- to test and evaluate the facility to verify the effective features as well as the level of safety.
- The nozzles were tested under extreme conditions to verify their heat resistance, and to detect any major problems in the flow fields downstream of the two mixer geometries. The flow along the nozzles was visualized using oil flow, and the thickness of the boundary layers was measured at the trailing edge using total pressure measurements,

- the main features of the flow field downstream of the lobe mixer and the “baseline” mixer were quantitatively outlined using total pressure surveys.

#### 4. 1. 1. Evaluation of the facility

To evaluate the facility, reacting flow conditions have been tested as well as cold flow conditions. The features tested include :

- the control of the gas supplies. All the commands were performed, and the reactions of the system were observed : the time response of the flowmeters, the ability of the flowmeters to maintain a given flow rate and the sensitivity of the indication of the flowmeters to the pressure at the exit of the bottles
- the safety system. The ignition system was tested, and a hydrogen regulator purge was performed. All the purge sequences were thoroughly checked.
- the effective range of flow rates. This was performed for cold flows by measuring the dynamic pressure obtained at the exit of the burner using an alcohol manometer. The velocities were then determined using eqn (2.11). The density of the alcohol was :

$$\rho_{alc} = 830 \text{ kg} \cdot \text{m}^{-3} .$$

For reacting flows, the flammability limits of the fuel were tested by varying the composition of the mixture and the flow conditions. The results are presented in Section 4. 2. 1.

- the ergonomics of the installation. In particular, the changes of nozzle and bottles were performed to look for possible improvements to the handling of the facility,
- the resistance of both mixer geometries to thermal stresses, as well as their main flow features. Reacting flow runs were performed, and the flow rates were varied over the full range specified in Chapter 2. The shape of the mixers was verified after each run to detect any deformations, which would indicate that the nozzles have failed. The flame was visible due to the impurities present in the air line. Therefore, the structure of the flow field was examined visually for both the lobed and the non-lobed geometries.

## **4. 1. 2. Examination of the flow along the nozzle**

To assess the performance of the lobed mixer, the flow field across the nozzle has to be examined. The main issue is to check the flow for any separation and to measure the actual boundary layer blockage to verify the turning of the flow obtained from the lobed mixer (i.e. the effective ramp angle showed on Figure 3.5). This goal was achieved by visualizing the flow in the troughs using oil flow visualization and by surveying the total pressure field at the trailing edge along a radius to estimate the thickness of the boundary layers.

Visualization of the flow of fluorescent oil along the walls of the mixer was conducted. The oil was colored by adding a fluorescent dry temp powder paint to it. The mixture was then applied on the wall, and the mixer was used under the desired flow conditions, which spread the oil along stream lines. The results of this visualization are presented in Section 4. 2. 2.

The total pressure surveys were conducted along a radial line at 0.02" downstream of the trailing edge. A Kiel probe was used to measure the total pressure. The internal diameter of the probe was 0.02". It was connected to the data acquisition system described in Section 4.1.3.b, with the only difference that the increment was chosen to be 0.02", in order to get a better resolution at the trailing edge. The results of these measures are presented in Section 4. 2. 2.

## **4. 1. 3. Survey of the flow field**

### **4. 1. 3. a. Experimental approach**

Once the examination of the flow along the nozzles was completed, the flow field from both the lobed and the non-lobed mixer was investigated. Total pressure measurements were implemented as a preliminary quantitative investigation. These time-averaged total pressure measurements provided information on the overall structure of the shear layer, through the variations of the time-averaged dynamic pressure across a horizontal cross-section. These variations are related through eqn (2.11) to the velocity of the flow as well as to the density of the mixture at the point of measurement.

In order to increase the contrast of the surveys and to reproduce the conditions that would be encountered in an hydrogen/air flow, a mixture of 60% helium and 40% nitrogen was used for the core flow in association with the air co-flow. Since no independent measure of the density of the gas was taken, no quantitative measure of the mixing rates was possible through those surveys. Besides, because of the turning imposed upon the flow by the lobed mixer (approximately  $\pm 20^\circ$ ), the indication of the pitot probe (which is fully accurate up to approximately  $\pm 15^\circ$ ) could only be used for qualitative observations.

Nevertheless, these surveys allowed for the structure of the shear layer to be examined in different flow conditions, as discussed in Section 4. 2. 3.

#### 4. 1. 3. b. Experimental apparatus

The facility used and the non-lobed mixer are described in Chapter 2. The lobed mixer is presented in Chapter 3. The pressure was measured using a pitot probe which specifications are :

- Internal diameter : 0.02",
- External diameter : 0.065".

The pitot probe was linked to a pressure transducer, which had the following specifications :

- Range :  $\pm 1$  inch of water ( $\pm 255 Pa$ )
- Output :  $\pm 10 V$
- Neutral point ( $P_{dyn} = 0 Pa$ ) :  $V_{out} = 5.45 V$
- Calibration curve :  $P_{dyn} = 57.534872 \times V_{out} - 316.08659 Pa$

The pitot probe was mounted on stepping motors to allow for a survey of a cross-section of the flow. Those motors were controlled by a PC-compatible computer through a Velmex NF90 controller connected to the serial port of the computer.

Data acquisition was performed using a A/D box connected to the data acquisition board of the computer. The software allowed the user to choose the number of steps in

each direction, the size of the increment in each direction, the number of measures to take in each point, and the waiting time between each step of the motors and the following data acquisition.

The following values were used :

- The time response of the data acquisition line was found to be approximately 3.5 seconds. Thus, to separate the measurements in two adjacent points, the waiting time before each measurement was chosen to be 4 s.
- The spatial increment was taken to be 0.04" in most cases. This value was chosen to allow the coverage of a sufficient area without increasing the time required to unacceptable levels. It also provided relatively good resolution, close to the best achievable with the pitot tube.
- 1000 measurements were taken at each point to obtain time-averaged values for each measurement.

The area surveyed is a quarter plane including the axis of the burner. In the case of the lobed mixer, it also included one full lobe. Because of the symmetry of the geometry, the flow field in the three other quarter planes is the same as that of the measured one. Hence a full cross-section can be reconstituted.

#### 4. 1. 3. c. Uncertainty

The uncertainty of the measure given by the transducer is of 1/2 count (the signal is measured on a scale from 0 to 4096 counts : -10 volts = 0 counts and 10 volts = 4096 counts). Thus, if  $V_{in}$  is the input of the computer, one can write :

$$V_{in} = \frac{N \times 20}{4096} - 10 \text{ volts} , \quad (4.1)$$

where N is the number of counts measured by the computer.

And using the calibration curve of the transducer :

$$P_{dyn} = 57.534872 \times V_{in} - 316.08659 \text{ Pa} . \quad (4.2)$$

Hence, the uncertainty of the measure is :

$$\Delta P = 57.534872 \times \frac{20}{4096} \times \frac{1}{2} = 0.14 Pa .$$

#### 4. 1. 3. d. Signal-to-Noise ratio

A preliminary run was performed with no flow, to measure the variations in the signal delivered by the data acquisition line. 100 measures were taken and statistically analyzed. The measure was unbiased, and the standard deviation of the signal was :

$$\sigma_{P_{dyn}} = 0.26 \text{ counts} = 0.07 Pa .$$

For a signal of 0.67 Pa (corresponding to a velocity of 4 m.s<sup>-1</sup> in hydrogen, i.e. the smallest expected signal), this yields a Signal-to-Noise ratio of 10.4%. For a signal of 75 Pa (11m.s<sup>-1</sup> in nitrogen), the Signal-to-Noise ratio is less than 0.1%.

## 4. 2. Results

### 4. 2. 1. Evaluation of the facility

The following remarks can be made concerning the operation of the facility :

- the flowmeters were found to allow a constant flow rate to be maintained with an accuracy of  $\pm 1\%$ . When submitted to a change in the flow rate commands, the flowmeter time response ranged between 1 s. to 10 s. Under certain conditions, such as a high nitrogen flow and a low hydrogen flow, the indication of flowrate became unstable, with variations of up to 100% on the desired value. This proved to be a problem during the evaluation of the flammability limits, since small and varying flow rates of hydrogen were added to high nitrogen flow rates.
- instead of a blue and almost invisible flame, the observations showed particles burning and emitting a yellow color. These particles came mostly from the air lines, since the density of yellow spots increased with the air flow rate. Fortunately, this problem decreased as large amounts of air were passed through the lines, which helped to clean the system. Nevertheless, the presence of these particles might create

a problem if laser diagnostics are to be used, since some optical diagnostics (e.g. Rayleigh Scattering) require a cleaner flame.

- as expected, the flame length was much shorter for the lobed mixer than for the non-lobed mixer under the same flow conditions (roughly 1/3 of the length). This shows the improved mixing associated with the use of the lobed geometry. The flow downstream of each individual lobe spread out more rapidly, and could be visually distinguished from the flow leaving the other lobes.
- the maximum velocities reached at the exit of the burner as well as the flow rates were estimated using a manometer which measured the dynamic pressure. Each gas supply was tested separately. For the hydrogen-helium lines, helium was used. The flow rates indicated by the hydrogen flowmeter had to be corrected since helium was being used. The corrections are discussed in Appendix D. The results are presented in Table 4.1.

	Air	Nitrogen	Helium
Indicated flow rate	n/a	300 SLPM	750 (*) SLPM
Measured dynamic pressure (Pa)	58.4	75.5	54.7
Measured velocity (m.s <sup>-1</sup> )	9.92	11.39	25.82
Estimated flow rate	310 SCFM	346 SLPM	785 SLPM

(\*) : corrected value

TABLE 4.1 : OPERATING RANGE OF THE FACILITY

Since the hydrogen is used under the same conditions (temperature and pressure) as the helium, the hydrogen flow rates are the same as the helium flow rates, as discussed in Section 2.2.1.a. Therefore, the velocities reached with hydrogen are the same as those reached with helium.

With a mixture of 50% hydrogen and 50% nitrogen, the maximum velocity reached was :

$$v_{3c} = 22.8 \text{ m.s}^{-1}$$

With a mixture of 86% helium and 14% nitrogen, the maximum velocity reached was :

$$v_{3c} = 30.0 \text{ m.s}^{-1}$$

For the fuel lines, the measured values were well over the design values. On the contrary, for the air line, the flow rate obtained was lower than the expected value. Nevertheless, the exit velocity reached in the co-flow is sufficient to test the mixers with a core flow to co-flow velocity ratio of approximately 0.4 (instead of the desired value of 0.3). The air flow rate is limited by the capacity of the compressed air line, which was running at its maximum, and by the pressure losses encountered in the air line.

- the flammability range of the hydrogen-nitrogen mixture was very broad. The flammability limit was determined by decreasing the hydrogen flow rate at constant air and nitrogen flow rates until the flame was blown off. The flammability limit was thus obtained as the minimum value of the hydrogen flow allowing a stable flame and was plotted, as showed in Figure 4.1.

The flammability limit did not vary significantly with the air speed and was approximately proportionnal to the nitrogen flowrate :

$$\dot{V}_{H_2 \text{ flame stability}} \cong \frac{1}{5} \dot{V}_{N_2} \quad (4.3)$$

Therefore, the lowest hydrogen molar fraction in the mixture providing a stable flame is :

$$x \cong \frac{y}{5} = \frac{1-x}{5} \text{ i.e. } x \cong 0.25 \quad (4.4)$$

This value is very close to the limit of flammability of hydrogen in the case of a premixed flame, which is around  $\phi = 0.2$ .

In addition, the use of the lobed mixer did not change significantly the flammability limits of the combustible mixture.



## **4. 2. 2. Examination of the flow along the lobed nozzle**

### **4. 2. 2. a. Oil flow visualization**

The use of this visualization method proved difficult to implement on the present geometry. Because of the vertically-standing burner position, the gravity prevented the oil from following the stream lines. No direct visualization of the stream lines was therefore possible. Nevertheless, the behaviour of the flow in the troughs on the core flow side of the lobes was visualized, and is shown on Figure 4.2.

This image shows a low-velocity area retaining some oil in the trough. This area could be a separation bubble caused by the transition between the non-lobed and the lobed section of the nozzle. Nevertheless, this phenomenon was more likely caused by pooling of oil than by boundary layer separation. The issue was resolved by examining total pressure surveys conducted to examine the boundary layers at the trailing edge of the mixers.

On the co-flow side of the nozzle, the flow was also surveyed for signs of separation using a thin thread attached to a wand. Even at low velocities, no sign of separation was detected.

### **4. 2. 2. b. Total pressure measurements**

Profiles of the total pressure at the trailing edge along the radial axis of a lobe are presented in Figure 4.3, Figure 4.4 and Figure 4.5. The measures were taken for a core flow of nitrogen at 14 m.s-1 and a co-flow of air at 10 m.s-1. From those plots, the boundary layer thickness at the trailing edge can be estimated for the lobed mixer for the troughs of both the core and the co-flow.

When expressed in terms of displacement thickness, these values yield thinner boundary layers than the estimate that was given in Section 3.3 :

	Lobed nozzle		Non-lobed nozzle	
	Core flow	Co-flow	Core flow	Co-flow
Boundary layer thickness	$\delta \cong 4.8 \times 10^{-3} m$	$\delta \cong 1.8 \times 10^{-3} m$	$\delta \cong 3.0 \times 10^{-3} m$	$\delta \cong 2.5 \times 10^{-3} m$
Displacement thickness	$\delta^* \cong 6.1 \times 10^{-4} m$	$\delta^* \cong 2.5 \times 10^{-4} m$	$\delta^* \cong 4.1 \times 10^{-4} m$	$\delta^* \cong 3.4 \times 10^{-4} m$

TABLE 4.2 : MEASURED BOUNDARY LAYER THICKNESS AT THE TRAILING EDGE

Therefore, the flow field that was measured here does not show any sign of separation. In addition, those results show that the estimate given in Section 3.3 for the boundary layer thickness is conservative.

Moreover, this tends to support the hypothesis that the low-velocity flow observed with the oil flow visualization is not a separation bubble but simply the oil pooling in the lobe trough due to gravity.

### 4. 2. 3. Qualitative survey of the flow field

Two different cross sections were surveyed to obtain qualitative information on the structure of the flow field downstream of the mixers : 1" and 2" downstream of the trailing edge. The core flow mixture was composed of 40% nitrogen and 60% helium. Both the non-lobed and the lobed mixer were tested, under 2 different flow conditions :

1.  $\begin{cases} v_{3_c} = 7.34 m.s^{-1} \\ v_3 = 9.92 m.s^{-1} \end{cases}$  i.e.  $r = \frac{v_{3_c}}{v_3} = 0.74$  , which gives  $\begin{cases} Re_{core} = 3.7 \times 10^5 \\ Re_{co} = 4.8 \times 10^5 \end{cases}$
2.  $\begin{cases} v_{3_c} = 6.96 m.s^{-1} \\ v_3 = 4.55 m.s^{-1} \end{cases}$  i.e.  $r = 1.53$  , which gives  $\begin{cases} Re_{core} = 3.6 \times 10^5 \\ Re_{co} = 2.2 \times 10^5 \end{cases}$

The pressure maps of the cross-sections presented in Figures 4.6 through 4.11 show the development of streamwise vortices forming at the tip of the lobes, and growing with the downstream distance. These mushroom-shaped structures, particularly visible on Figure 4.6, grow rapidly and then decay. By comparing Figure 4.7 with Figure 4.6 and Figure 4.10 with Figure 4.9, one can see that those structures decay rapidly with the

downstream distance. On Figure 4.9, the vortices forming from each wall of the lobe seem to be separated from each other.

The results also show the increased interfacial area provided by the lobed geometry. The enhanced mixing from the lobed geometry is also visible when comparing the situations at  $z=2''$  between the lobed and non-lobed mixers. The pressure field is more homogeneous in the case of the lobed mixer, with less accentuated contrasts in the pressure field across the cross-sections. This indicates that the two co-flowing streams have mixed more in the case of the lobed mixer.

Comparing those results to the total pressure measurements conducted by Underwood on a planar lobed mixer [36], one finds that for  $z=2''$  (corresponding to roughly 2.5 lobe wavelength downstream of the trailing edge), the mixing seems more thorough in the case of the axisymmetric mixer. This can be explained by the fact that due to the axisymmetric geometry, the streamwise vortices forming from two adjacent lobes are farther apart. Therefore, those vortices can diffuse longer before interfering and cancelling each other. Since the enhanced mixing is provided by this diffusion of the vorticity, the mixing rate is higher in the case of the axisymmetric mixer.

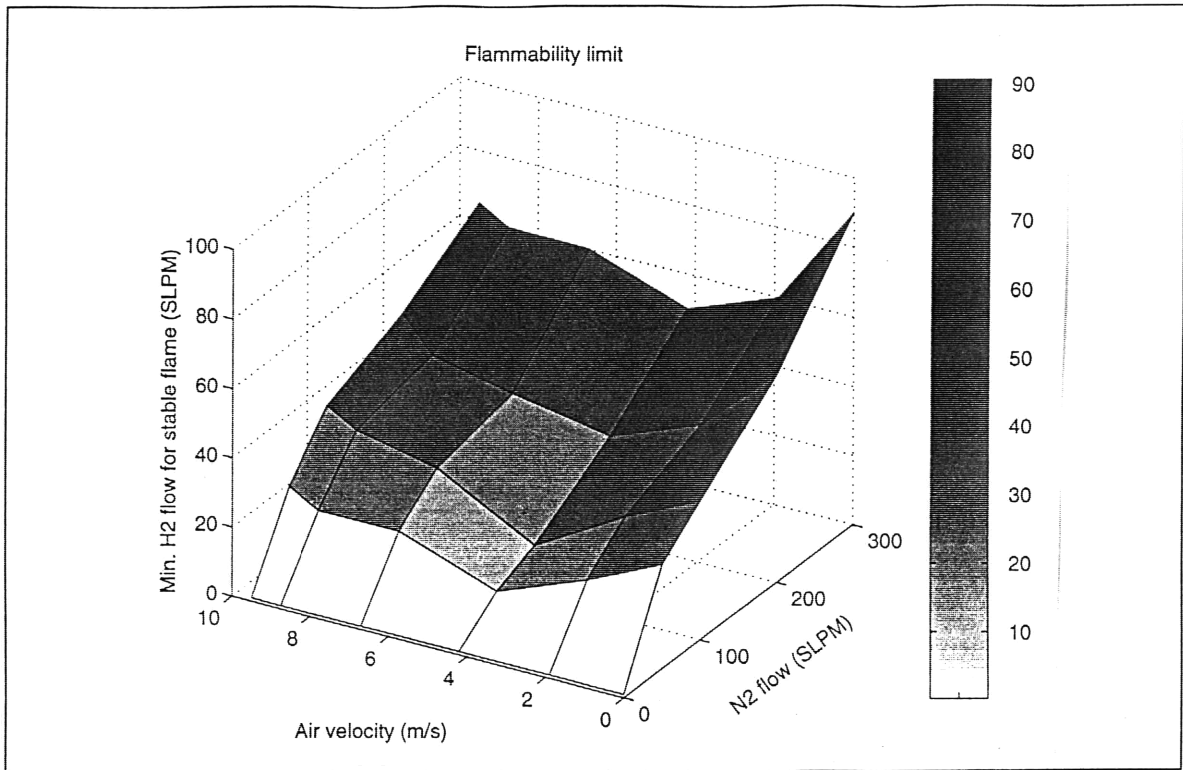


FIGURE 4.1 : FLAMABILITY LIMIT

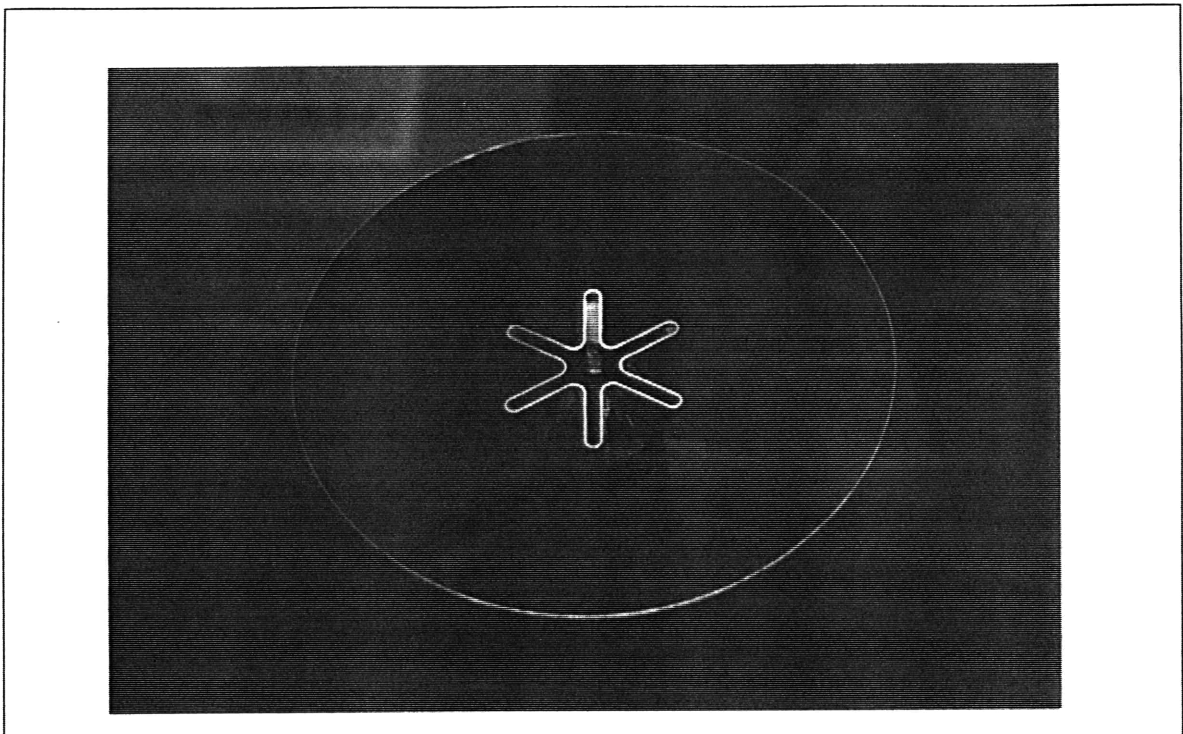


FIGURE 4.2 : OIL FLOW VISUALIZATION OF THE CORE FLOW AT 15 M.S<sup>-1</sup> (PARTIAL VUE)

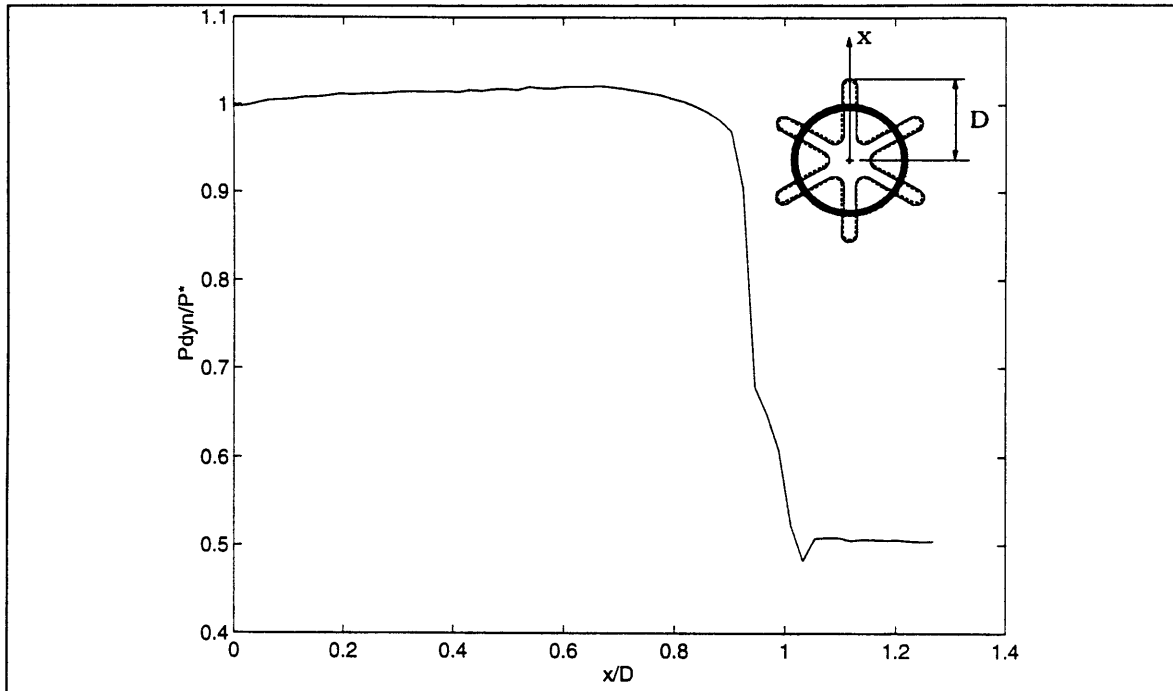


FIGURE 4.3 : TOTAL PRESSURE ALONG THE RADIAL AXIS OF AN EXTERNAL LOBE, AT 0.02" DOWNSTREAM OF THE TRAILING EDGE, LOBED MIXER  $r=1.4$ .

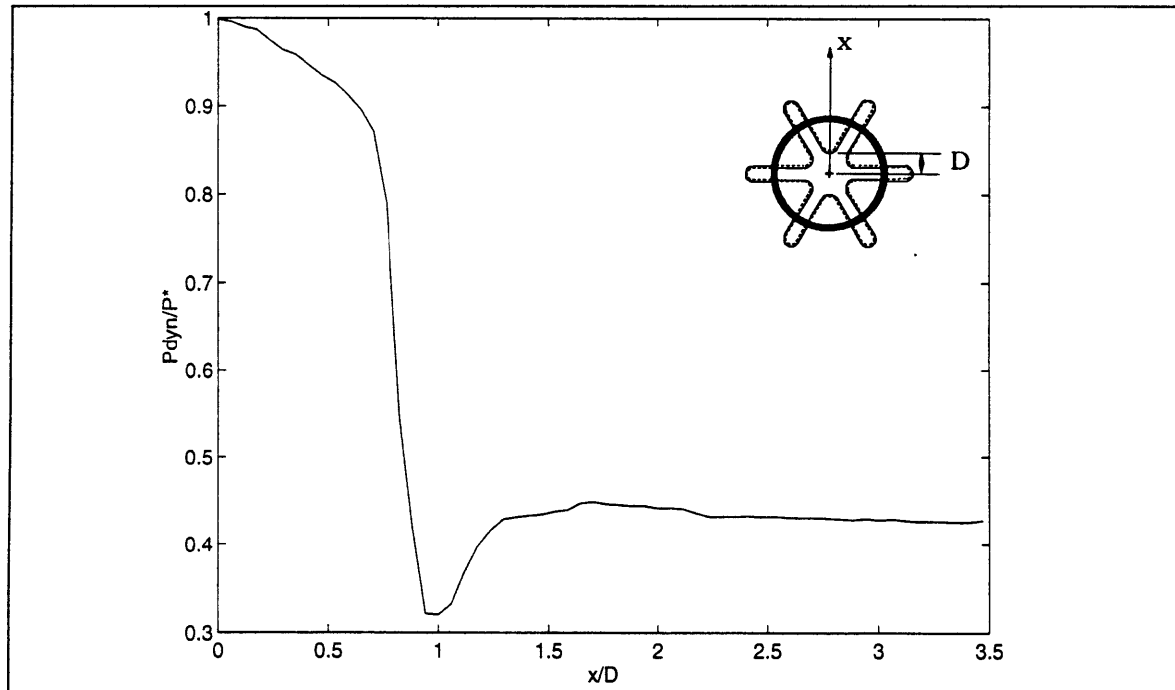


FIGURE 4.4 : TOTAL PRESSURE ALONG THE RADIAL AXIS OF AN INTERNAL LOBE, AT 0.02" DOWNSTREAM OF THE TRAILING EDGE, LOBED MIXER  $r=1.4$ .

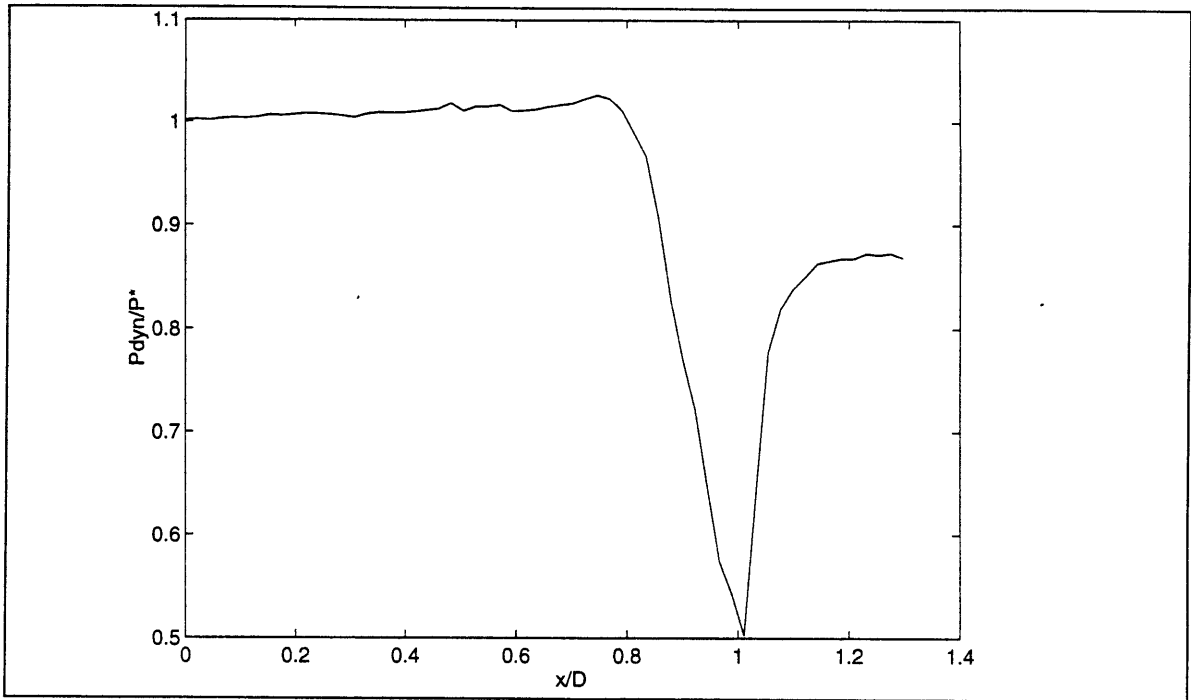


FIGURE 4.5 : TOTAL PRESSURE ALONG A RADIUS, AT 0.02" DOWNSTREAM OF THE TRAILING EDGE, NON-LOBED MIXER,  $r=1.4$ .

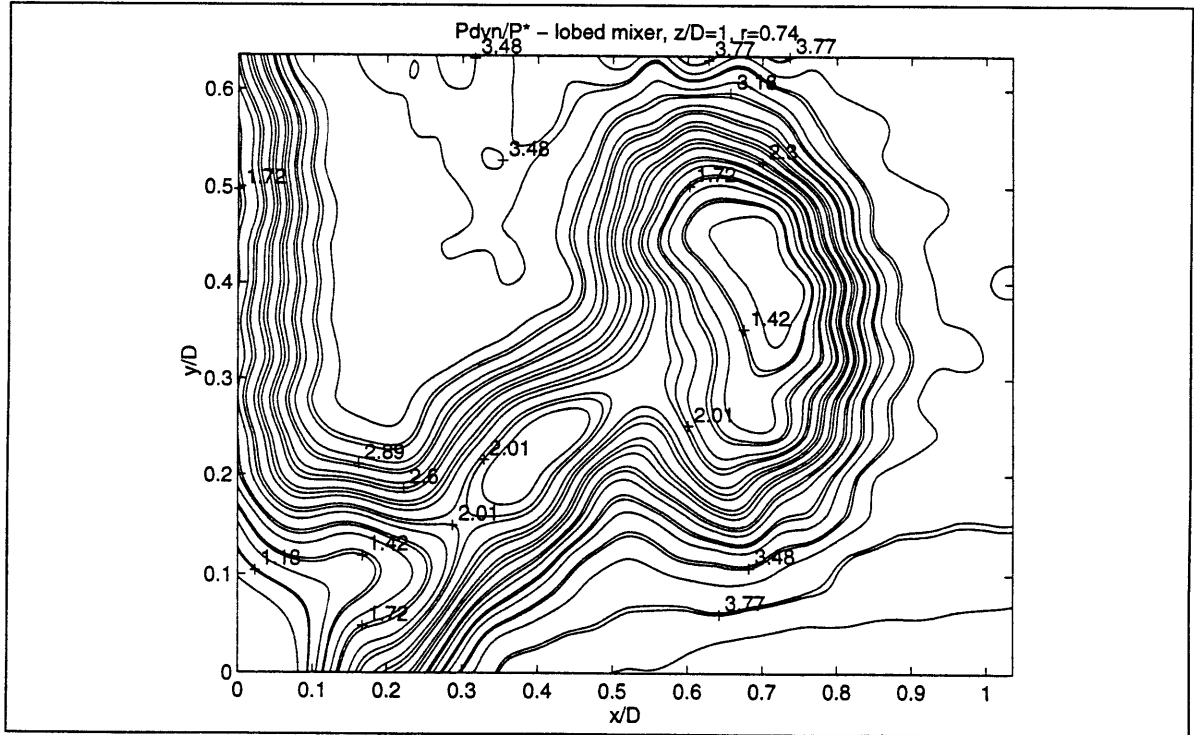


FIGURE 4.6 : DYNAMIC PRESSURE, LOBED MIXER AT  $Z=1''$  FOR  $r=0.74$

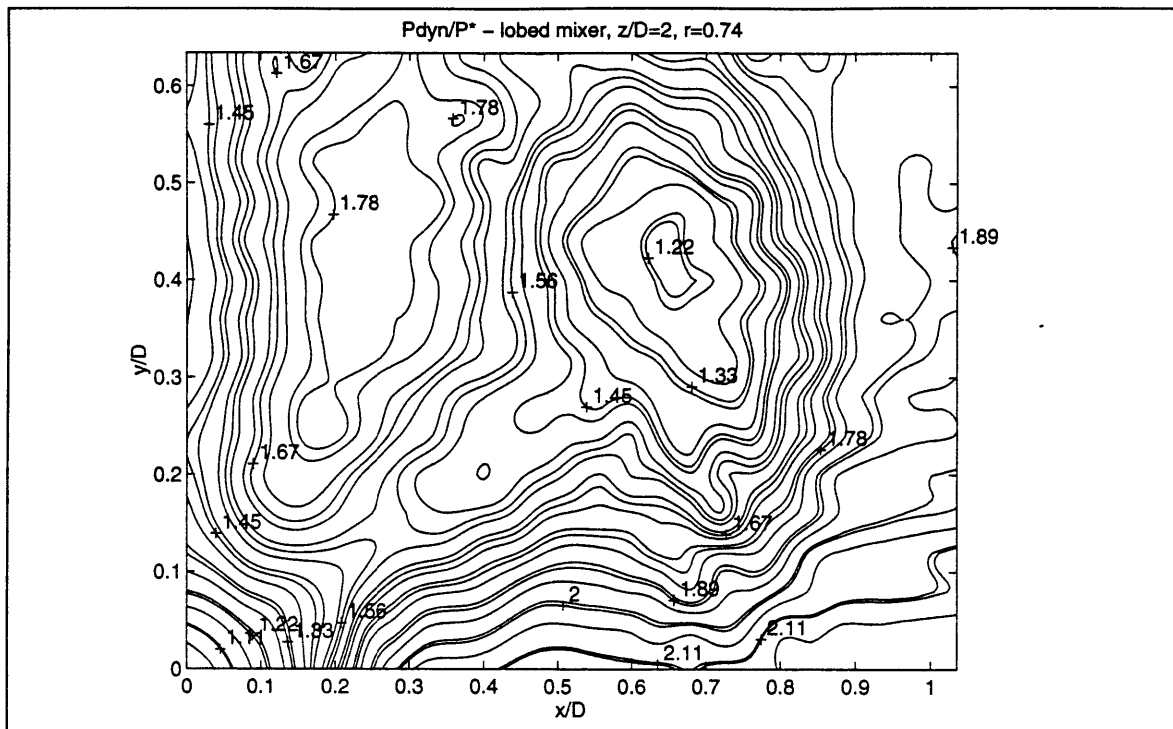


FIGURE 4.7 : DYNAMIC PRESSURE, LOBED MIXER AT Z=2" FOR r=0.74

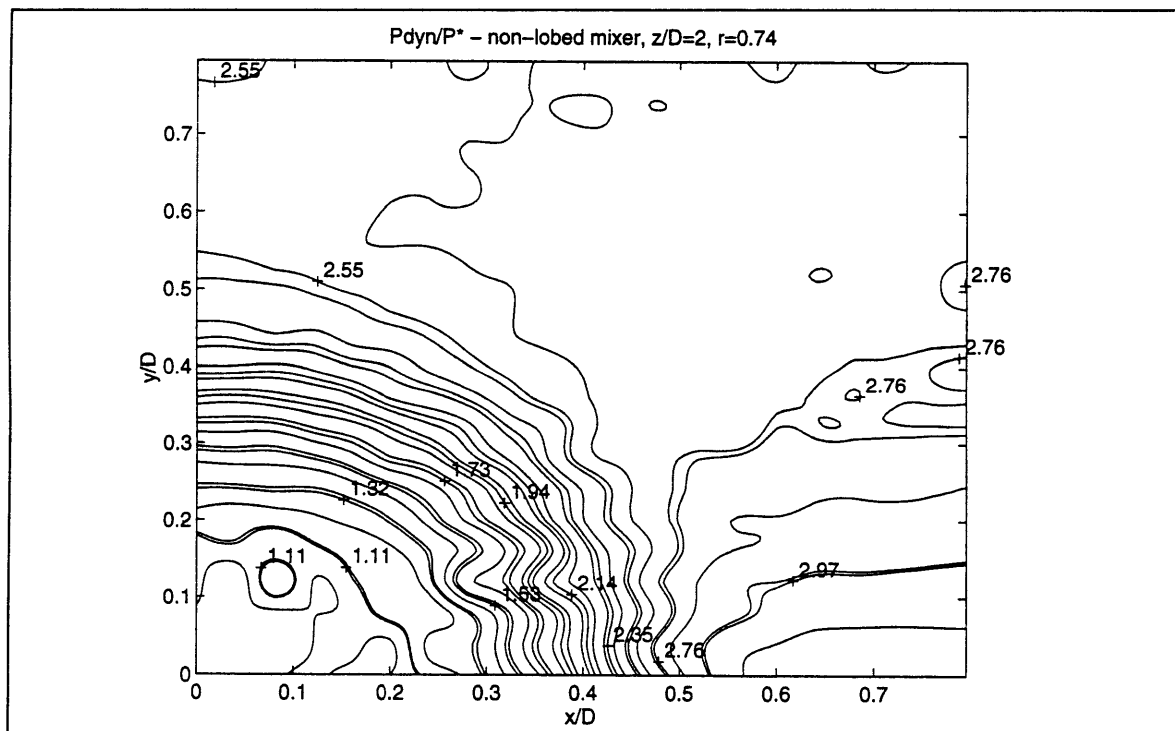


FIGURE 4.8 : DYNAMIC PRESSURE, NON-LOBED MIXER AT Z=2" FOR r=0.74

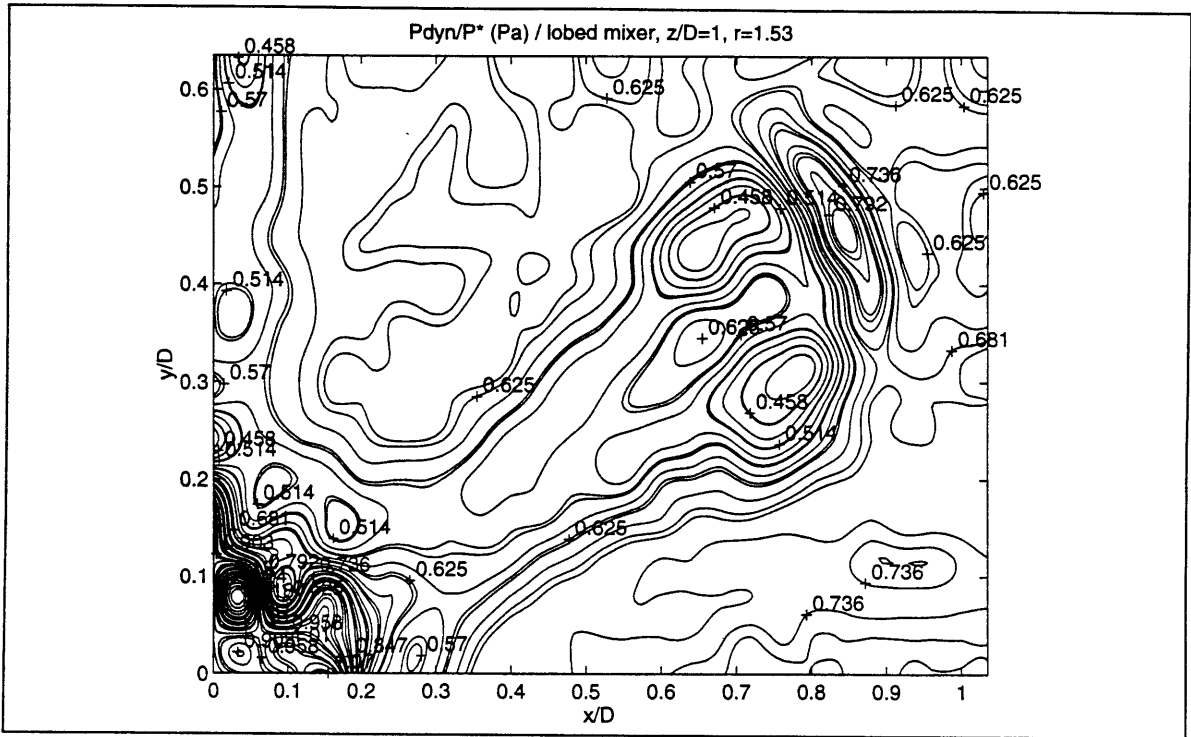


FIGURE 4.9 : DYNAMIC PRESSURE, LOBED MIXER AT Z=1" FOR r=1.53

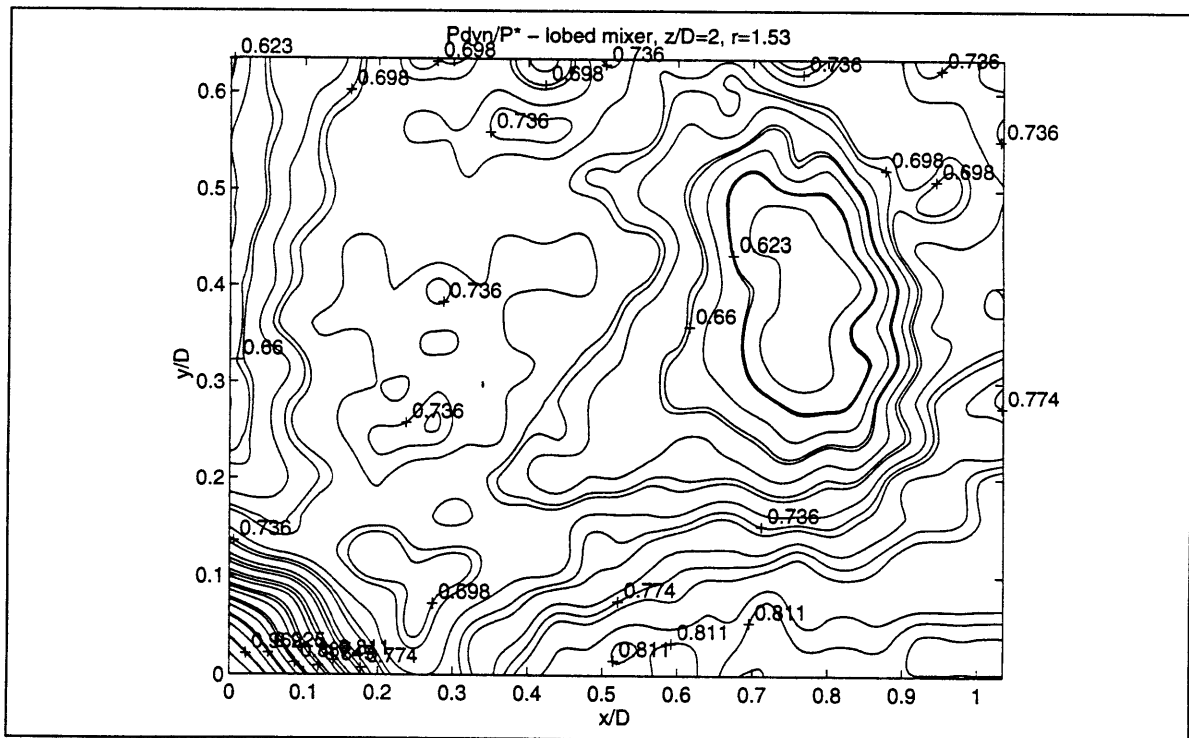


FIGURE 4.10 : DYNAMIC PRESSURE, LOBED MIXER AT Z=2" FOR r=1.53



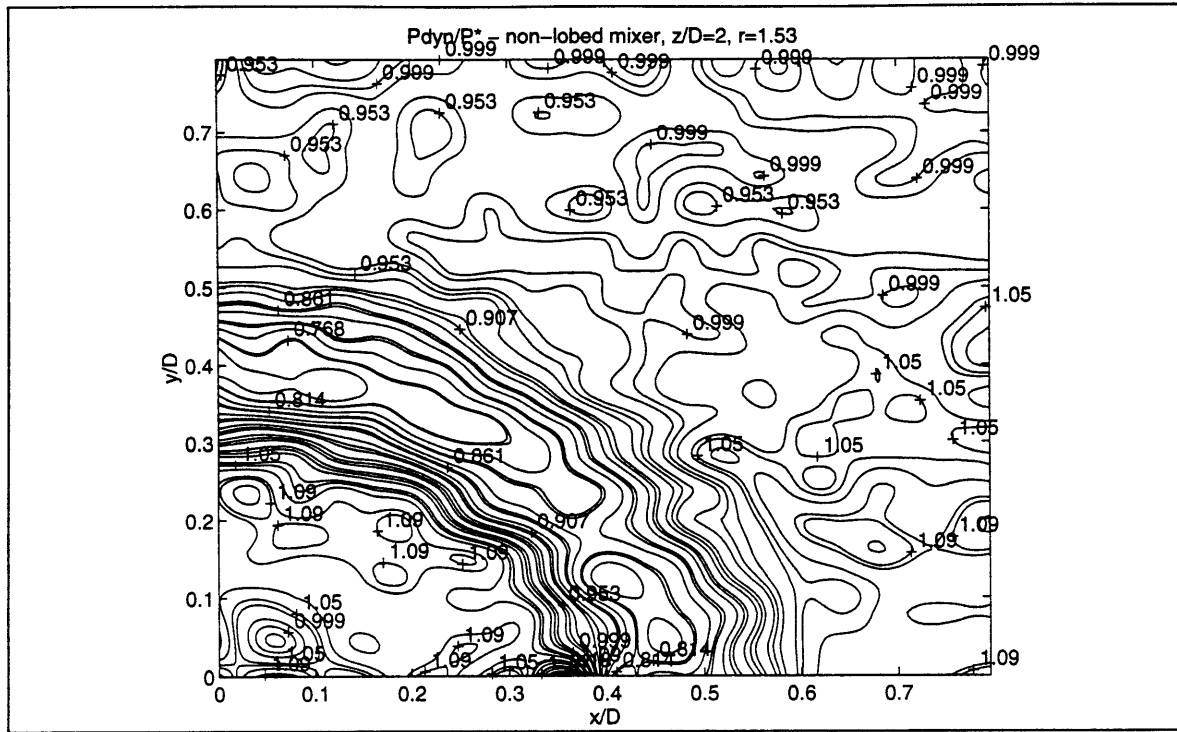


FIGURE 4.11 : DYNAMIC PRESSURE, NON-LOBED MIXER AT  $Z=2''$  FOR  $r=1.53$



# 5. Conclusions and Recommendations

The modified facility now provides an effective means of testing the performance of axisymmetric lobed mixers, with a high level of safety and reasonable handling ergonomics.

Nevertheless, the following improvements should be made to the facility :

- the ignition system used (described by McGrath [16]) should be equipped with a longer arm which would retract farther away from the flame region., in order to leave more space for future surveys of the flow,
- the compressed gas cabinet could be used to stock two hydrogen bottles linked together by a manifold, in order to provide longer test times. The nitrogen bottle could simply be secured outside of the gas cabinet,

The surveys that were conducted upon the flow field about the lobed mixer showed that the design goals were reached. Namely, the boundary layer thickness and the thermal stresses were found to be within the limits set by the design. The qualitative survey of the flow downstream of the lobed mixer showed the mixing enhancement provided by the lobed nozzle. In particular, the roll-up due to the streamwise vorticity was observed.

The following recommendations relate to the use of the facility to test lobed mixers :

- The first step to take could be to measure the mixing rate downstream of the lobed mixer, using total pressure surveys. This could provide a more accurate determination of the actual performance of the mixer.
- Diagnostics with shorter time response and higher spatial resolution could then be implemented on both reacting and non-reacting flow fields. Among those, the use of ionization probes should provide useful information about the behaviour of the flame front.
- Nevertheless, the present situation seems most suitable for laser diagnostics : first, the flow being turbulent, optical diagnostics will provide the time resolution necessary to conduct instantaneous surveys of the flow. Second, most laser diagnostics can be used for both the cold and the reacting flows. This should prove a major asset when investigating the difference introduced by the heat release.

# References

- [1]: Anderson B., Povinelli L., Gerstenmaier W., *Influence of Pressure Driven Secondary Flows on the Behavior of Turbofan Forced Mixers*, AIAA-80-1198, 1980
- [2]: Barber T., Paterson R.W., Skebe S.A., *Turbofan Forced Mixer Lobe Flow Modeling : Part I - Experimental and Analytical Assessment*, NASA CR4147, 1988.
- [3]: Becker H.A., Liang D., *Visible Length of Vertical Free Turbulent Diffusion Flames*, Comb. Flame, vol. 32, 1978, pp. 115-137.
- [4]: Belovitch V.M., Samimy M., Reeder M.F., *Dual Stream Axisymmetric Mixing in the Presence of Axial Vorticity*, AIAA-94-3084, 1994.
- [5]: Bernal L.P., Roshko A., *Streamwise Vortex Structure in Plane Mixing Layers*, Journal of Fluid Mechanics 170, pp. 499-525, 1986.
- [6]: Birch S.F., Paynter G.C., Spalding D.B. and Tatchell D.G., *An Experimental and Numerical Study of the 3-D Mixing Flows of a Turbofan Engine Exhaust System*, AIAA-77-0204, 1977.
- [7]: Candel S., *Mécanique des Fluides*, cours de 2ème année, Ecole Centrale Paris, 1992.
- [8]: Elliot J.K., *A Computational Investigation of the Fluid Dynamics of a Three-Dimensional, Compressible, Mixing Layer with Strong Streamwise Vorticity*, Master's thesis, Massachusetts Institute of Technology, 1990.

- [9]: Elliot J.K., Manning T.A., Qiu Y.J., Greitzer E.M., Tan C.S., Tillman T.G., *Computational and Experimental Studies of Flow in Multi-Lobed Forced Mixers*, AIAA-92-3568, July 1992.
- [10]: Frost T.H., *Practical Bypass Mixing Systems for Fan Jet Aero Engines*, *Aeronautical Quarterly*, v.17, pp. 141-161, 1966.
- [11]: Kozlowski H., Kraft G., *Experimental Evaluation of Exhaust Mixers for an Energy Efficient Engine*, AIAA-80-1088, 1980.
- [12]: Krasnodebski J.K., Personal Communication, Aero-Environmental Research Laboratory, 1995.
- [13]: Krasnodebski J.K., O'Sullivan M.N., Waitz I.A., Greitzer E.M., Tan C.S., *A Computational Study of Viscous Effects on Lobed Mixer Flow Features and Performance*, manuscript in preparation, Massachusetts Institute of Technology, 1995.
- [14]: Manning T.A., *Experimental Studies of Mixing Flows with Streamwise Vorticity*, Master's thesis, Massachusetts Institute of Technology, 1991.
- [15]: McCormick D.C. and Bennett J.C., *Vortical and Turbulent Structure of a Lobed Mixer Free Shear Layer*, AIAA-93-0219, 1993.
- [16]: McGrath P.J., *Design and Testing of a Facility to Study Mixing Augmentation in Reacting Flows*, Master's thesis, Massachusetts Institute of Technology, 1995.
- [17]: Michel R., Quémard C., Cousteix J., *Méthode pratique de prévision des couches limites turbulentes bi et tridimensionnelles*, *La Recherche Aérospatiale*, n° 1972-1.
- [18]: Mills A.F., *Heat Transfer*, Irwin, Boston, 1992.
- [19]: Paterson R.W., *Turbofan Mixer Nozzle Flow Field - A Benchmark Experimental Study*, *J. Eng. Gas Turbines and Power*, vol. 106, pp. 692-698, 1984.
- [20]: Povinelli L.A., Anderson B.H., Gerstenmaier W., *Computation of Three Dimensional Flow in Turbofan Mixers and Comparison with Experimental Data*, AIAA-80-0227, 1980.

- [21] : Presz W.,Gouzy R., Morin B., *Forced Mixer Lobes in Ejector Designs*, AIAA-86-1614, 22nd. Joint Combustion Conference (1986).
- [22] : Presz W. Jr., Blinn R.F., *Short Efficient Ejector Systems*, AIAA-87-1837, 1987.
- [23] : Qiu Y.J., *A Study of Streamwise Vortex Enhanced Mixing in Lobed Mixer Devices*, Master's thesis, Massachusetts Institute of Technology, 1992.
- [24] : Schlichting H., *Boundary Layer Theory*, Seventh Edition, McGraw-Hill, New York, 1979.
- [25] : Taine J., *Transferts Thermiques*, Bordas, Paris, 1989.
- [26] : Tew D.E., *A Computational Study of Mixing Downstream of a Lobed Mixer with a Velocity Difference Between the Co-Flowing Streams*, Master's thesis, Massachusetts Institute of Technology, 1992.
- [27] : Tew D.E., Personal Communication, Aero-Environmental Research Laboratory, 1995.
- [28] : Timoshenko S., *Theory of Elasticity*, New York, 1934.
- [29] : Truckenbrodt E., *Ein Quadraturverfahren zur Berechnung der laminaren und turbulenten Reibungsschicht bei ebener und rotationssymmetrischer Strömung*, Ing.-Arch. 20, pp. 211-228 (1952).
- [30] : Truckenbrodt E., *Neuere Erkenntnisse über die Berechnung von Strömungsgrenzschichten mittels einfacher Quadraturformeln*. Part 1 : Ing.-Arch. 43, pp. 9-25 (1973) ; Part 2 : Ing.-Arch. 43, pp. 136-144 (1974).
- [31] : Underwood D., *Effect of Heat Release on Streamwise Vorticity Enhanced Mixing*, Master's thesis, Massachusetts Institute of Technology, 1995.
- [32] : Waitz I.A., Underwood D.S., *Effect of Heat Release on Streamwise Vorticity Enhanced Mixing*, AIAA 95-2471, 1995.
- [33] : Werle M.J., Paterson R.W. and Presz Jr., *Flow Structure in a Periodic Axial Vortex Array*, AIAA-87-0610, 1987.

[34] : Wieghardt K., *Turbulente Grenzschichten*, Göttinger Monographie, Part B5 (1945-1946).



# Appendix A : New instrumentation and hardware specifications

## Two Way Direct Acting Solenoid Valve (for the 1/2" lines)

Description : ASCO Red-Hat II, Model EF 8210 G2

Specifications : Connections : 1/2" NPT female  
Body material : brass  
Orifice size : 5/8"  
Cv flow factor : 4  
Max. operating Pressure Differential : 200 psi  
Electrical connections : 120 volts, AC, 60 Hz.  
Explosion proof.

## Mass Flow Controller (for the hydrogen and nitrogen flows)

Description : Hastings Model HFC-203

Specifications : Range : 0-500 SLPM for hydrogen and 0-300 SLPM for nitrogen  
Connections : 1/2" Swagelok  
Body material : 316 stainless steel  
Control valve pressure differential : 10-50 psi  
Pressure rating : 500 psi  
Accuracy & linearity : ± 1%  
Power : ± 15 VDC @ ±50mA/-200mA  
Electrical connections : 15 pin D connector.

## **Orifice Plate Mass Flowmeter (for the air flow)**

Description : Hastings Model HOP-2C

Specifications : Range : 0-500 SCFM of air  
Connections : 2" Male NPT  
Body material : 316 stainless steel  
Control valve pressure differential : psi  
Pressure rating : psi  
Accuracy & linearity :  $\pm 1\%$   
Power :  $\pm 15$  VDC @  $\pm 50$ mA / -200mA  
Electrical connections : 15 pin D connector.

## **Check Valve (for the 1/2" lines)**

Description : Circle Seal Model 259B-4PP

Specifications : Max. flow : 0-30 SCFM of air  
Connections : 1/2" Female NPT  
Body material : brass  
Control valve pressure differential :  $\cong 20$  psi @ 30 SCFM  
Pressure rating : 3000 psi

## **Particle Filter**

Description : Matheson Model 6134-T8FF (for nitrogen) and 6124-T8FF (hydrogen)

Specifications : Max. flow : 0-400 SLPM (nitrogen) and 0-500 SLPM (hydrogen)  
Connections : 1/2" Swagelok  
Body material : 316 stainless steel  
Purity : 100% filtration efficiency at 0.2 micron level

## **Pressure Regulator**

Description : Matheson Model 3020 /580 (for nitrogen) and 3020 /350 (hydrogen)

Specifications : Max. flow : 0-2200 SLPM  
Connections : 1/4" NPT Female  
Body material : 316 stainless steel

# Appendix B : Boundary layer growth along the nozzle

Parameters		Fuel	
b	0.1520	% N2	14.0%
beta	0.0127	% H2	86.0%
c	4.0000	viscosity N2 (kg/m.s)	1.757E-05
		viscosity H2 (kg/m.s)	8.870E-06
<b>Air</b>		rho (N2) (kg/m3)	1.165
viscosity (kg/m.s)	1.80E-05	rho (H2) (kg/m3)	8.380E-02
rho (kg/m3)	1.2	viscosity fuel (kg/m.s)	1.009E-05
Air Flow (m3/s)	0.2223	rho (fuel) (kg/m3)	0.235
		Fuel Flow (m3/s)	7.600E-03

	Co-Flow (Air)			Core Flow (H2+N2)		
	Section 1	Section 2	Section 3	Section 1 core	Section 2 core	Section 3 core
<b>Area (m2)</b>	0.03721	0.01672	0.01482	1.947E-03	5.910E-04	5.066E-04
<b>Speed (m/s)</b>	5.97	13.30	15.00	3.90	12.86	15.00
<b>(m)</b>	0.525	0.706	0.728	0.525	0.706	0.728
<b>R3(x)</b>	937.5658	4.851E+02	n/a	260.2751	1.267E+02	n/a
<b>G(x)</b>	32.7489	6.874E+01	n/a	12.2841	4.010E+01	n/a
<b>N(x)</b>	1.465E+09	1.601E+09	n/a	5.2864E+06	5.072E+07	n/a
<b>H(x)</b>	1.0000	4.5687E+00	n/a	1.0000	6.1107E+00	n/a
<b>H23(x)</b>	0.5557	0.5067	n/a	0.5557	0.5059	n/a
<b>H12(x)</b>	1.2869	1.0277	n/a	1.2869	1.0243	n/a
<b>Momentum thickness (m)</b>	2.354E-03	5.473E-04	1.642E-03	2.860E-03	4.228E-04	1.268E-03
<b>Displacement thickness (m)</b>	1.683E-03	2.850E-04	8.551E-04	2.046E-03	2.191E-04	6.572E-04



# Appendix C :Thermal stresses, complete results

Parameters				
Velocity (in m/s)	15	(0.02")	thermal conductivity H2 (in W/m/K)	1.98E-01
Downstream dist. of exit section (in m)	0.686		thermal conductivity N2 (in W/m/K)	2.67E-02
thermal conductivity gas (in W/m/K)	1.363E-01		rho (H2, in kg/m3)	8.38E-02
thermal conductivity steel (in W/m/K)	39.37		rho(N2, in kg/m3)	1.165
Cross-sectional thickness (in m)	5.08E-04		visc.(H2, in kg/m.s)	8.87E-06
Tadiab. (in K)	2400		visc.(N2, kg/m.s)	1.76E-05
Lobe length (H, in m)	0.0219		% H2	64%
Young's modulus (steel) (in psi)	2.80E+07		% N2	36%
Poisson's coef.	0.27		rho(fuel, in kg/m3)	0.473032
Coef. of therm. expansion (in 1/K)	1.73E-05		visc.(fuel, in kg/m.s)	1.200E-05

Results				
Re(z=zmax)	4.06E+05	(must be << 0.25)	Air temp. away from flame (in K)	
h	1.754E+02		To= 300	
Biot's number	2.264E-03		T(z)=A.(exp(mz)-exp(-mz))+To	
<b>Temperature profile in the lobes</b>			m= 187.3136517	
z (height, in m)	0.0219		A= 0.806713787	
T(z) (in K)	349			
Temp. Gradient (in K)	49			
	(Timoshenko)			
<b>MAX THERMAL STRESS (in psi)</b>	<b>2.36E+04</b>		<b>ELASTIC LIMIT (in psi)</b>	<b>6.00E+04</b>



# Appendix D : Corrections on helium flow rates

In order to make cold flow measurements, the hydrogen was replaced by helium. Therefore, the flowmeters being calibrated for hydrogen, the flow rate indication is going to be biased, and corrections have to be made to obtain the actual flow rate.

The properties of helium at standard conditions are :

$$\begin{cases} \mu_{He} = 2.01 \times 10^{-5} \text{ kg} \cdot \text{m}^{-1} \cdot \text{s}^{-1} \\ \rho_{He} = 1.624 \times 10^{-1} \text{ kg} \cdot \text{m}^{-3} \\ k_{He} = 0.149 \text{ W} \cdot \text{m}^{-1} \cdot \text{K}^{-1} \end{cases}$$

The flowmeters which are installed on the lines are thermal meters, i.e. they measure the flow rate through the estimation of the heat transfer to the fluid flowing through them :

$$\dot{V}_{indicated} \propto \frac{1}{h} , \quad (\text{D.1})$$

where  $h$  is the heat transfer coefficient from the sensor to the fluid.

Since the heat transfer is accomplished by forced convection, one can use eqn. (3.28) and (3.32) to estimate  $h$  :

$$h = \frac{k}{z} Nu_z = \frac{0.0288k}{z} Re_z^{1/2} Pr^{1/4} . \quad (\text{D.2})$$

Therefore, assuming that  $Pr=1$  for both gases, the ratio of the indicated flow rates is :

$$\frac{\dot{V}_{He}}{\dot{V}_{H_2}} = \frac{h_{H_2}}{h_{He}} = \frac{k_{H_2}}{k_{He}} \left( \frac{\rho_{H_2} \cdot \mu_{He}}{\rho_{He} \cdot \mu_{H_2}} \right)^{4/5} \quad (D.3)$$

Replacing the viscosities and densities in eqn. (D.3), one finds :

$$\frac{\dot{V}_{He}}{\dot{V}_{H_2}} = 1.133 \times \frac{k_{H_2}}{k_{He}} = 1.506$$

2556-28